# Optical/Near-Infrared Observations of Infrared-Excess Palomar-Green QSOs

Jason A. Surace

SIRTF Science Center, MS 314-6, California Institute of Technology, Jet Propulsion Laboratory, Pasadena, CA 91125; and University of Hawaii, Institute for Astronomy, 2680 Woodlawn Dr., Honolulu, HI, 96822

Electronic mail: jason@ipac.caltech.edu

D. B. Sanders

University of Hawaii, Institute for Astronomy, 2680 Woodlawn Dr., Honolulu, HI, 96822

Electronic mail: sanders@ifa.hawaii.edu

Received _____; accepted _____

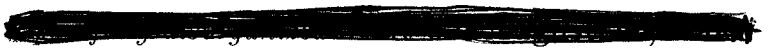

## ABSTRACT

Ground-based high spatial-resolution (FWHM $< 0.3$–$0.8''$ ) optical and near-infrared imaging at BIHK′(0.4—2.2 $\mu$m) is presented for a complete sample of optically selected Palomar-Green QSOs which have infrared excesses at least as great as those of "warm" AGN-like ultraluminous infrared galaxies ($L_{ir}/L_{blue} > 0.46$). In all cases, the host galaxies of the QSOs were detected and most have considerable two-dimensional structure. One-half of the QSOs occur in spiral hosts while an additional one-quarter show extended merger-induced tidal tails suggestive of mergers between similar-sized disk galaxies. Eleven percent are in elliptical hosts, and the remainder are indeterminate. Slightly more than half of the spiral hosts have strong nuclear bars or other nuclear disturbances consistent with (but not necessarily implying) very advanced minor merger systems, bringing the possible merger fraction to as high as 50%. Several of the systems have knots of star formation similar to those seen in other merger systems and in the ULIGs. H-band luminosities of the hosts range from 0.4-7.5 $L^*$ with a mean of 2.2 $L^*$, and are also consistent with those found in ultraluminous infrared galaxies. This result suggests that some, but not all, optically-selected QSOs may have evolved from an infrared-active state.

*Subject headings:* quasars: general—galaxies: active—infrared: galaxies

## 1. Introduction

Since their initial discovery thirty-five years ago, quasi-stellar objects (QSOs) have been the subject of enormous debate. Chief among these has been the question of what mechanism is the source of their enormous luminosities. The observed short-period variability of QSOs, the appearance of collimated radio jets in radio-loud quasars, and the presence of broad emission lines all helped drive the "standard model" of QSO structure, namely one involving accretion disks surrounding supermassive black holes. However, the size-scale of the accretion disk is relatively small, and it is difficult to drive new material at the required rate into the nucleus from the rest of the galaxy; this problem is known commonly as "feeding the monster" (Gunn 1979).

Early n-body experiments by Toomre & Toomre (1972) had suggested that galaxy collisions might be able to bring large supplies of material deep into their central regions. Additional theoretical work has helped support this picture (Hernquist 1989, Bekki & Noguchi 1994, Barnes & Hernquist 1996). Many other studies have implicated various kinds of galaxy interactions as being important to nuclear activity. Stockton & MacKenty (1987) demonstrated directly the presence of merger activity (in the forms of bridges and other extended emission) in a considerable fraction of QSO host galaxies. More recent *HST* results, as well as many ground-based studies, have similarly provided direct evidence of interactions and mergers (Bahcall et al. 1997, Hutchings et al. 1995, Kukula et al. 1997, 1998, Dunlop et al. 1993). A large body of evidence indicates that even minor interactions alone, and not actual mergers, can fuel QSO activity, since the rate of companion galaxies in close proximity to QSOs is abnormally large (Yee 1987, Lake et al. 1998). Some workers have even taken this idea one step further with the claim that perhaps the interactions are all that are required and that an interaction induced super-starburst can produce at least the radio-quiet QSO phenomenon without invoking black holes at all (Terlevich 1989).

Since an understanding of the QSO phenomena seems to hinge critically on understanding the fueling mechanism, much attention has turned to the environment in which the quasar nucleus is presumably embedded. It has long been known that Seyfert active nuclei resemble lower-luminosity optical QSOs in many ways, and are additionally the nuclei of galaxies. Indeed, the distinguishing feature often used to differentiate QSOs and Seyfert galaxies was the morphological difference that QSOs appeared primarily stellar and did not appear to be embedded in luminous galaxies (Schmidt & Green 1983). Since that time, increasing numbers of observations from the ground have demonstrated to the contrary the presence of extended emission around QSOs apparently compatible with being galaxies (Hutchings et al. 1984, Gehren et al. 1984, Neugebauer et al. 1987). More recent imaging from the ground, particularly in the near-infrared, has begun to investigate in detail the galactic environments of QSOs (Hutchings & Neff 1992, McLeod & Rieke 1994a,b, Kukula et al. 1997).

Many galaxies (e.g., Seyfert galaxies, radio galaxies) also have forms of abnormally energetic behavior lumped under the general heading of active galactic nuclei (AGN). IRAS discovered a new class of these AGN: galaxies that had QSO-like bolometric luminosities ($L_{\rm bol} > 10^{12}\ L_{\odot}$) yet which emitted nearly all of their luminosity at far-infrared wavelengths. Many of these galaxies show evidence for merger activity along with optical line ratios similar to that of other AGN (Sanders et al. 1988, Murphy et al. 1996, Veilleux et al. 1999). Tying together the theoretical framework for merger-induced fueling along with an evolutionary timeline, Sanders et al. (1988) proposed that these so-called ultraluminous infrared galaxies (ULIGs) were the immediate progenitors of optically selected QSOs, and that ULIGs represented a stage in QSO evolution where the active nuclei were enshrouded in gas and dust. This dust shroud reradiates the nuclear emission at far-infrared wavelengths; eventually, powerful winds (Heckman et al. 1990) disperse the dust and reveal an optical QSO nucleus. An understanding of these objects would therefore greatly advance theories

of QSO evolution.

Surace & Sanders (1998;1999), Surace et al. (2000a; 2000b), and Scoville et al. (2000) explored the morphology and colors of the circumnuclear and extended environments of ULIGs at optical and near-infrared wavelengths. They demonstrated the presence of a compact core at near-infrared wavelengths, whereas the emission at optical and near-ultraviolet wavelengths the ULIGs are dominated by an extended starburst many kpc in size. If QSOs are relic ULIGs, then their host galaxies should provide evidence for the structures found in ULIGs: extended tidal tails and debris, and aged star-forming knots from a tidally-triggered starburst.

Traditionally, the greatest impediment to detecting QSO host galaxies has been the relatively low surface brightness of the galaxies relative to the QSO nucleus. Under typical ground-based seeing conditions (FWHM $\approx$ 1– 1.5″) and with typical detectors (particularly with photographic methods), the glare (residual PSF contamination due to seeing and scattered light) from the QSO nucleus has been sufficient to obscure the host galaxies. One of the prime motivators of *HST*, equipped with modern CCD detectors and possessing 10–20 $\times$ the spatial resolution of ground-based instruments (at optical wavelengths), was to image QSO hosts. Ironically, the early results from these projects have been mixed at best, and contradictory at worst. Early reports indicated that many of the observed QSOs had no detectable hosts with limits of typically 1 $L^*$ (Bahcall et al. 1995), which was surprising in light of earlier studies and was immediately contradicted by ground-based follow-ups (Neugebauer et al. 1995, McLeod & Rieke 1995). Subsequent additional *HST* imaging showed the presence of detectable hosts, but seemed to indicate that they existed in such a diverse number of environments that it was unclear if any common environment existed (Bahcall et al. 1997).

This apparent state of confusion motivated a new ground-based high spatial resolution

study of nearby optically-selected QSOs in order to provide a new, uniform set of imaging data to investigate the questions opened by the *HST* controversy. By observing a complete sample with properties similar to those of ULIGs and using the same instruments and techniques as Papers I-IV, the question of the relationship between the structure of the QSO hosts and the host galaxies of ULIGs can be investigated. The development of high quantum efficiency, large format detectors spanning the wavelength range from the near-ultraviolet to the near-infrared meant that a detailed study could be carried out over a wide range of wavelengths dominated by different emission processes. The advent of adaptive optics techniques coupled with superior ground-based sites also meant that this imaging could be carried out with much higher spatial resolution than ever before possible, making detection of QSO host galaxies and any compact features within them much easier.

We report the results of an imaging survey at B, I, H, and K′-band of a complete sample of low redshift ($z< 0.16$) QSOs selected from the Palomar-Green Bright Quasar Survey (Schmidt & Green 1983) on the basis of having an infrared-excess at least as great as that of "warm" ULIGs and which therefore are a possible evolutionary link between ULIGs and optical QSOs. Their morphology, luminosity, and colors are compared to those of the ULIGs (Surace et al 1998, Surace & Sanders 1999), and the implications for the ULIG- QSO evolutionary scenario are discussed.

## 2. Data

### 2.1. Sample

Sanders et al. (1988) proposed a possible evolutionary scenario by which ULIGs evolved into optical QSOs. In this scenario the "warm" ULIGs represent a more evolved form of ULIGs, similar to QSOs based on the presence of high ionization Seyfert emission lines.

The goal of the selection of this sample was to further the refinement of this evolutionary sequence by isolating a set of quasars which are more similar to the ULIGs than optical QSOs in general, and hence are likely to be in a younger evolutionary state.

The sample is drawn from all Palomar-Green Bright Quasar Sample ( PG; Schmidt & Green 1983) QSOs with redshifts $z \gtrsim 0.16$, thus placing them in the same space volume as the "cool" and "warm" ULIG samples examined by Surace et al. (1998) and Surace et al. (2000a). This is important because the interpretation of galaxy morphology often depends on the achieved physical spatial resolution. For example, the large "knots" in NGC 4038/9 seen from the ground are revealed by HST to be composed of smaller subclumps of star forming clusters. By examining the sample with the same techniques used in Paper III, the morphology is likely to be interpreted in a similar fashion. Additionally, the low redshift of the sample has the advantage that as the closest examples of their populations they are the most amenable to detailed study.

In order to search for transition objects which might bridge the gap between "warm" ULIGs ($f_{25}/f_{60} > 0.2$) [1] and the general QSO population an infrared selection criterion was imposed. Only those PG QSOs with infrared excesses (compared to the luminosity in the "big blue bump") at least as high as those of the warm ULIGs were selected. This was characterized by the ratio $L_{ir}/L_{blue}$ [2] , where these two quantities were computed from the data given by Sanders et al. (1989). The ULIG with the lowest such value is 3C273, which has $L_{ir}/L_{blue} = 0.46$. Therefore, only PG QSOs with $L_{ir}/L_{blue} > 0.46$ were selected. The

---

[1]The quantities $f_{12}$, $f_{25}$, $f_{60}$, and $f_{100}$ represent the *IRAS* flux densities in Jy at 12 $\mu$m, 25 $\mu$m, 60 $\mu$m, and 100 $\mu$m respectively.

[2]$L_{\rm ir} \equiv L(8--1000\mu{\rm m})$ is computed using the flux in all four *IRAS* bands according to the prescription given in Perault (1987). $L_{\rm blue}$ is computed from the luminosity at 3200–8400Å and a correction of 0.7 (Sanders, private communication)

distribution of $L_{ir}/L_{blue}$ for this QSO sample and ULIGs is not the same, nor could they be, given that ULIGs by definition almost always have much greater values of $L_{ir}/L_{blue}$. This criterion was only selected to search for "red" QSOs which might have significant dust content and hence be more similar to ULIGs than other QSOs.

Ideally, the QSOs would have the same distribution of bolometric luminosities as the ultraluminous infrared galaxies since it is hypothesized that the infrared luminosity in ULIGs is QSO-driven. In practice this is actually difficult to achieve. Besides being well-studied, the PG QSO sample was the only one at the time of this project with well-characterized far-IR emission. The PG BQS has too few objects meeting both our redshift and infrared color criterion to allow the construction of a meaningfully large sample with the same bolometric luminosity distribution as the ULIGs. Possibly, future studies could avoid this problem by using other infrared QSO surveys, such as those undertaken by ISO (Hooper et al. 1999) or SIRTF. Therefore, the QSO sample was selected instead to meet the same minimum bolometric luminosity criterion for ULIGs, namely $L_{bol} > 10^{12} L_{\odot}$. The bolometric luminosity was determined in two ways. First, $L_{bol}$ was estimated from $L_{bol}$ =16.5 $\times \nu L_B$ where $L_B$ is the luminosity at B-band, which is the average bolometric correction found for PG QSOs by Sanders et al. (1989). Under this definition the luminosity $L_{bol}$=$10^{12}$ $L_{\odot}$corresponds to $M_B$=-22.18. Papers identifying ULIGs have principally used a different cosmology than Schmidt & Green (e.g. $H_0$=75 km $s^{-1}$ mpc $^{-1}$ vs. 50 km $s^{-1}$ mpc $^{-1}$), adjusting for this implies that QSOs have $M_B$ < -23, similar to the definition found in that paper. Second, where possible $L_{bol}$ was determined directly from the data of Sanders et al. (1989). Since $L_{bol}$ for UGC 5101 is slightly below $10^{12} L_{\odot}$, the range in bolometric luminosities was allowed to drop to Log $L_{bol}$=11.92. Two objects in our sample (PG 1126-041 and PG 1229+204) were included because of this.

There are 17 infrared-excess PG QSOs, out of a total of 36 candidates meeting the

redshift and bolometric luminosity criterion. However, 3 of these (I Zw 1, Mrk 1014, and 3c273) are also "warm" ULIGs and have already been discussed in detail in Papers I and II. One additional QSO was observed (PG 1119+120). Although it falls just short of our luminosity criterion ($M_B$=-22.71), it has historically been considered a QSO (Neugebauer & Matthews 1999, Rowan- Robinson 1995).

It is worth noting that there is a strong morphological selection bias built into the Palomar-Green Survey. In particular, the survey states that a QSO " ...should have a dominant starlike appearance on blue prints of the 48 inch (1.2 m) Schmidt Sky Atlas..." (Schmidt & Green 1983). This criterion was then used to distinguish between QSOs and Seyfert galaxies. Objects which might have shown broad lines but had particularly luminous host galaxies were thus discarded as Seyfert 1s. This criterion was then further used to create the $M_{\rm B}$ <-23 luminosity criterion used to define QSOs, as most of the objects below this criterion showed evidence for nebulosity, but those above did not. However, this criterion is flawed; numerous studies have shown that typically the QSO nucleus and its host galaxy are of comparable luminosity (McLeod et al. 1994ab), although this is wavelength dependent. Therefore, distant objects measured through large apertures might meet the luminosity criterion due to the presence of their host galaxies. Additionally, lower redshift objects whose nuclei might meet the luminosity criterion but whose host galaxies are also very bright and/or extended will be rejected. In short, the PG BQS is biased against QSOs with luminous extended hosts at low redshifts. This morphological bias is likely to skew the results of this study towards finding systems with low luminosity hosts and towards hosts with few recognizable features. Other studies (Goldschmidt et al. 1992, Kohler et al. 1997) have also indicated quantitatively that the BQS is incomplete and heavily biased. In particular, it seems to be incomplete by at least a factor of 2 for low redshift, low luminosity QSOs ($z$< 0.3; $-23 > M_{\rm B} > -24.1$). Any results found here regarding the fractions of QSOs with luminous, extended (and possibly with interacting morphologies) hosts are thus likely

to be underestimates of the true fraction. On the other hand, Kohler et al. (1997) also finds that the space density of high luminosity QSOs has been severely underestimated in the BQS. Finally, under the unified model there should exist "Type II" QSOs whose geometry is such that the QSO nucleus is hidden from view by the obscuring dust torus, and evidence has been found for a sizable population of red QSOs entirely missed by optical QSO surveys (Webster et al. 1995). The results presented here, particularly in regards to what fraction of the QSO population has what properties, should therefore be interpreted strictly in the light of our sample selection criteria. The question of their relevance to the general QSO population, whatever that might be, may have to wait until a better understanding of the space density of physical objects called "QSOs" is achieved.

### 2.2. Observations and Data Reduction

The optical data were taken at the f/31 focus of the University of Hawaii 2.2m telescope using a fast tip/tilt guider in the same manner as described previously by Surace & Sanders (1999) and Surace et al. (2000a). B & I-band data were acquired with the Tektronix 2048 and Orbit 2048 cameras between May 1996 and December 1997. In most cases this was by direct imaging at the f/31 Cassegrain focus. In these cases, the data were binned on chip 2x2, yielding adopted pixel scales of 0.14 and 0.09″, respectively. In a few cases the data were obtained by reimaging the f/31 beam at f/10 through the HARIS spectrograph using the Orbit 2048 camera, yielding a pixel scale of 0.14″. While the fast tip/tilt guider is not capable of appreciably correcting atmospheric seeing at optical wavelengths, it can eliminate common-mode vibrations such as wind shake, which contribute appreciably to image degradation. Typical spatial resolutions varied between 0.4— 0.9″. Total exposure times varied between 12 and 54 minutes. Individual exposure times were short enough to prevent saturation of the QSO nucleus. In some cases the Cassegrain focus was rotated in

order to improve offset guidestar acquisition, in which case additional flat-field images were taken at the appropriate rotations.

The optical data reduction involved several steps. First, the CCD bias pattern was removed by subtracting from each image a high S/N median bias frame constructed from sequences of 20-30 bias frames at the beginning and end of each night. Pixel-to-pixel response variations were then corrected by dividing each image by a high S/N flat produced by making dithered observations of the twilight sky in each filter. Typical twilight exposures were 2-3 seconds each; short enough to avoid getting detectable flux from field stars, yet long enough to avoid flat-field errors introduced by the radial shutter used at the UH 2.2m. Estimated S/N for the flats (based on Poisson statistics and the gain of the CCD) was between 250-500. Neither CCD showed any evidence of measurable dark current, based on an examination of long closed shutter exposures. The images were then corrected to normal orientation by transposition and rotation using the ROTATE task in IRAF based on the known field rotation of the Cassegrain focus of the UH 2.2m, which is accurate to better than 1 degree. The CCD overscan regions were trimmed using IMCOPY. The images were then aligned using the IMALIGN task in IRAF, which uses a marginal centroiding routine that calculates a best fit solution to a number of (user-supplied) reference stars in the field. Typical alignment errors were estimated (on the basis of the fit) to be about 0.25 pixels. Given that the data was typically sampled at 5 pixels FWHM for a point source, alignment errors are unlikely to be important. The images were then averaged using an algorithm that rejects pixels inconsistent with the known noise properties of the CCD, which allows for rejection of cosmic rays. The shifted images were combined onto a larger image than the original data frames, thereby increasing the total field of view due to the dithering process. This was valuable primarily in order to increase the availability of PSF stars, since the camera field of view was much larger than the measurable extent of any of the galaxies.

The near-infrared H & K′ data were acquired between August 1996 and January 1998 with the QUIRC $1024^2$ HgCdTe camera (Hodapp et al. 1996) at the UH 2.2m using the f/31 Cassegrain focus and the tip/tilt guider. At this focus the plate scale is 0.06 $''$pixel$^{-1}$. The K′ filter was chosen due to the lower thermal background and hence greater sensitivity (Wainscoat & Cowie 1992). Throughout this paper we exclusively refer to K′. Comparison to work by other authors is made using the conversion of Wainscoat & Cowie (1992). In all cases exposure times were short enough (60–240 seconds) to prevent saturation of the QSO nucleus, thus allowing PSF subtraction during post-processing. Typical achieved spatial resolution using tip/tilt was 0.25— 0.5$''$. Total exposure times varied from 9 to 45 minutes per filter. Details of the new observations presented in this paper are given in Table 1.

The near-infrared data were reduced in the same manner as that described in Paper II. The data was initially sky-subtracted using consecutive, dithered frames; because the QUIRC field of view is so large (32$''$), it was possible to dither the target on-chip, thereby increasing telescope efficiency by a factor of 2. The images were then flattened using median flats constructed from images of the illuminated dome interior. Each image was then masked by hand to exclude bad pixels and regions contaminated by negative emission introduced by the sky subtraction. Images were aligned using the method described above for the optical data. Images were scaled according to their exposure times and then, in order to account for any variable sky background, an offset was subtracted from each image based on the background actually measured in that frame. The images were then combined by medianing using IMCOMBINE and rejecting pixels outside the linear regime of the array.

One QSO, PG 1202+281, could not be observed as there were no guide stars sufficiently bright ($m_V < 13$) and nearby ( $radius < 5'$) to enable the use of the tip/tilt guider. This QSO was, however, observed by *HST*/WFPC2. Several other QSOs (PG 1229+204, PG

1402+261, and PG 2130+099) have also been observed with *HST*/WFPC2 as part of other observing programs (Hutchings & Morris 1995, Bahcall et al. 1997), and were available through the STScI archival retrieval system. The WFPC2 images were generally taken through the F606W and F702W filters which correspond roughly to V and R- band, and are therefore not directly comparable to our data. They are, however, valuable for interpreting morphology that is only marginally resolved in our ground-based imaging. This data was acquired from the *HST* archive and reduced in the same manner as described by Surace et al. (1998); i.e., by shifting and rotating according to the astrometric solution provided by STScI, and combined using the GCOMBINE task in IRAF/STSDAS, with cosmic ray-rejection. Residual glitches were interpolated by hand using IMEDIT. The three PG QSOs which are also warm ULIGs (I Zw 1, Mrk 1014, and 3c273) have also been observed with *HST* (Surace et al. 1998, Bahcall et al. 1995); since this data appears elsewhere in the literature, it is not presented here.

The ground-based data were flux calibrated using observations of Landolt and Elias standard stars in the optical and near-infrared ( Landolt 1983,1992, Elias et al. 1982). In most cases the nights were photometric with $\sigma_{\rm M} < 0.05$. For data taken on non-photometric nights, we have calibrated the data by using large fixed-aperture photometry already in the literature for the targets. Specifically, the near-infrared data for PG 0007+106 and PG 1001+054 were calibrated using the photometry given in Neugebauer et al. 1987 and the magnitude zeropoints contained therein. Optical data for PG 1119+120, PG 1440+356, PG 1613+290, and PG 2130+099 were calibrated using the photometry of Neugebauer et al. (1987) and the magnitude zeropoints of Bessel (1979). Photometric calibration errors are 0.03 magnitudes. For additional discussion of photometric errors as a result of measurement see §3.2.

The point-spread-function (PSF) was calibrated by using actual stars in the final

combined science images using DAOPHOT in the manner described in Paper II. All of the stars were identified, scaled, shifted, and combined using a sigma-clipping algorithm and weighted according to total flux, thus creating as high a S/N PSF image as possible. In those few cases where no stars were found in the science images, the PSF was estimated by using the closest temporally adjacent PSF. Since the tip/tilt guiding has little effect on atmospheric distortions at short wavelengths, this works well for optical data. Similarly, since the seeing remains stable on timescales of many minutes, this is also effective in the near-infrared. For the *HST*/WFPC2 data, theoretical PSFs were calculated using the TinyTim software (Krist 1994). The PSFs were important in determining the photometry since they provided all of the needed aperture corrections.

Unlike some authors, no attempt is made to fit models to the surface brightness distributions of the QSO host galaxies in an attempt to classify them as spiral or elliptical-like. The interpretation of radial profiles is fairly ambiguous (Surace & Sanders 2000). The differences between the de Vaucoleurs profile and the exponential disk profile are most unambiguous at small radii. However, the surface brightness distribution at small radii is dominated by the QSO nucleus, and incomplete knowledge of the PSF prevents the recovery of sufficient information about the host at these radii. Instead, we consider the operative definition that elliptical galaxies have predominantly smooth surface brightness distributions. High surface brightness, high spatial frequency non-radially symmetric structure (such as spiral arms) are the surest sign that something is not an elliptical galaxy. Pre-supposing that QSO hosts are ellipticals, which will be further reinforced by the blurring effects of atmospheric seeing, forces this analysis to err in assigning elliptical-like properties to too many QSO hosts.

# 3. Results

## 3.1. Morphology

### *3.1.1. Large-Scale Features*

Host galaxies (as evidenced by extended emission beyond that expected for a point source) were detected in every QSO system observed. Their morphology is surprisingly diverse. Figure 1 presents the large-scale morphology of all the QSOs (except I Zw 1, Mrk 1014, PG 1202+281, and 3c273) at all four observed wavelengths. In each case the images have been stretched in an attempt to emphasize the faint structure in the host galaxies. Figure 2 presents the optical data for every QSO including I Zw 1 and Mrk 1014 for completeness but excluding PG 1202+281 and 3c273 as near-truecolor images (we have no optical data for these two objects). These images are the most intuitive to understand and hence the most instructive for the following discussion (Surace et al. 2000a).

Of the 18 QSOs, 9 clearly lie in spiral galaxies based on the presence of spiral arms or rings and bars (including I Zw 1). An additional 4 (including Mrk 1014) have clear major merger morphologies with long tidal arms which strongly hint at disk progenitors. Two galaxies are known to be ellipticals: 3c273 and PG 1202+281 (Bahcall et al. 1997). McLeod et al. (1994b) claim a detection for the latter but give no information on spatial structure. The remainder (PG 1001+054, PG 1351+640, & PG 1415+451) are indeterminate and lack any obvious structure in their extended emission. These three indeterminate cases also have very high nuclear luminosity fractions, thus making them hard to classify. Our morphologies generally agree well with existing published data (Hutchings & Neff 1992, Dunlop et al. 1993, McLeod et al. 1994ab) . Adopting the criteria for radio "loudness" of $P_{5GHz} > 10^{24.7}$ watts $Hz^{-1}$ (Woltjer 1990) and the radio fluxes of Kellerman et al. (1994), we find that all of our sample QSOs are radio-quiet except for 3c273. Since as many as

76% of the radio-quiet QSOs in our sample occur in spiral hosts, this seem to support earlier claims that radio-quiet QSOs occur most often in spirals, and contradicts some recent claims that elliptical hosts are more predominant (Bahcall et al. 1997). The only radio-loud object, 3c273, is known to have an elliptical host. This may be a result of the way the sample was selected: our QSO sample was chosen specifically to have an infrared excess. It is known that infrared-selected samples of galaxies are biased strongly against ellipticals; for example, elliptical galaxies are vastly under-represented in *IRAS* surveys, presumably due to a lack of dust (Sulentic 1988, Surace 1998). Also, this may point to the morphological type being a function of luminosity. McLure et al. (1999) find that all of the QSOs they observed lie in elliptical-type hosts. However, those QSOs had $M_R > -23.1$ (adjusted for cosmology), which is more luminous than the majority of our sample.

Five hosts have strong nuclear bars ranging from 10–22 kpc in length. These thick bars may have been detected previously and been thought to be elliptical hosts; deeper imaging reveals spiral arms and rings attached to them. The fraction of barred systems (56% 5/9) is higher (by roughly a factor of 2×) than that usually found for intermediate-type field spirals and early-type spirals found in the field or in groups (Elmegreen et al. 1990).

Four host galaxies (including Mrk 1014) have tidal tails and arms and are unmistakably recent merger systems. Thus, at least 22% (4/18) of the far- infrared excess PG QSOs occur in merger systems. This is similar to the ≈15% interaction fraction found by Bahcall et al (1997). Moreover, Hutchings et al. (1992,1994,1995) classified PG 1229+204 as a merger involving a small companion resulting in the observed bar and ring structures. Hutchings & Neff (1992) also propose that PG 2130+099 may also be in a post- interaction state, although it is not clear if it's disturbed morphology necessarily implies merger activity. None of the four merger systems with obvious tidal tails is one of the barred systems. It is possible that the barred systems are also merger remnants. Laine & Heller (1999) have

shown that the merger of a spiral galaxy and a much smaller companion can produce a barred morphology similar to that seen in the IR-excess PG QSOs. However, these "minor" mergers are qualitatively different from the "major" mergers which involve similarly massive galaxies. Counting the 5 barred spirals and the 4 merger systems, interactions of some kind may be implicated in as many as 50% of the QSOs.

### *3.1.2. Star-Forming Knots*

Compact high surface brightness emission regions are detected in 33% (6/18) of the QSO hosts. In particular, "knots"[3] of star formation like those found by the ULIGs (Surace et al. 1998,1999) are detected in PG0007+106, I Zw 1, Mrk 1014, PG 1119+120, PG 1229+204, PG 1411+442 and PG 1613+658. Four of these are also the same systems that show evidence for merger activity; a fifth is also postulated to be a merger remnant (Hutchings & Neff 1992). The remaining QSO (PG 1119+120) shows evidence for a very red off-nuclear knot, as well as several very blue knots embedded in structure of the outer arms.

Figure 4 shows some of the small scale-scale nuclear structure, enhanced by a variety of techniques. The optical data for I Zw 1 and Mrk 1014 appear in Figure 2, while the near-infrared data appear in Paper II. The structure in PG 1119+120 is clearly seen in Figure 1. In most cases the observed PSF had insufficient S/N to be used for a high quality point source subtraction and so a noiseless model of the QSO nucleus was used instead. In Figure 4 radial profile models have been fit to the QSO nuclei using the ELLIPSE and BMODEL routines in IRAF/STSDAS. The models were forced to be circular, with

[3]"knots" are defined as closed isophotes less than 1 arsecond in radius and 3 $\sigma$ above the surrounding emission.

centers fixed on the QSO nuclei. They were then subtracted from the raw data, leaving only the non-radially symmetric component of the QSO host galaxy behind. Even with this technique, structure within a radius of 1–2″(2–4 kpc) of the nucleus generally cannot be recovered at optical wavelengths due to confusion with subtraction artifacts arising due to pixel aliasing. In the near- infrared the situation is considerably better, as illustrated by the detection of the "jet"-like feature in PG 1411+442. Unfortunately, the host galaxies have much less structure at these wavelengths. In several cases a modified version of this technique was used. Radial profile models were fit using the JIP imaging package in a manner similar to that above; only in this case the fitting region for the radial models was restricted to specific position angles, allowing exclusion of obvious structure such as stars. This results in a more accurate model which has less tendency to oversubtract from the host galaxy. The nuclear subtracted I-band image of PG 0007+106 clearly shows an arc or tidal tail similar to that in Mrk 231. The nuclear-subtracted image of PG 1229+204 shows the galactic bar, as well as the condensations both in the bar and near its ends. The data for PG 1411+442 at I-band show a north-south structure extending both to the north and south of the nucleus. Since the northern extension seems to be the base of the tidal tail, it is possible the southern structure is actually the base of a fainter counter-tail. There are many bright condensations or knots in the northern tail itself. The close-up image to it's right shows the bright knot (or possibly jet-like) feature to the southwest. The bottom two panels show PG 1613+658. On the left is the nuclear-subtracted wide-field image, showing the long tidal tail to the east and what appears to be a counter-tail extending west. The right hand panel shows a deconvolved K′ image of the nuclear regions. To the northeast is the bright nuclear knot described by Hutchings & Neff (1992). Additionally, there is a less luminous high surface brightness region to the southwest.

### 3.2. Luminosities

Table 2 lists BIHK′ integrated photometry for all of the QSOs as well as nuclear and host galaxy luminosities and nuclear fractions. The integrated photometry was derived by measuring the total flux of the QSO/host system in an aperture large enough to encompass the optical extent of the galaxy at a flux level below 1 $\sigma$. Measurement errors from this technique are small and are dominated by the photometric calibration errors. The host galaxy luminosity was then derived by subtracting the contribution of the QSO nucleus and any high surface brightness features (e.g., star forming knots). As in Paper II, the luminosity of the QSO nucleus was determined in two ways: measuring the flux in a fixed 2.5 kpc radius aperture and then correcting this with an aperture correction derived from the observed PSF, and also by fitting the observed PSF to the nucleus such that a smooth host galaxy flux distribution without holes resulted. Generally, these results were the same to within 10%. This is not surprising; since the surface brightness of the QSO nucleus is much higher than that of the underlying galaxy, small aperture photometry will mostly be sensitive to the QSO nucleus as the underlying host contributes only a small fraction of the total flux inside the aperture. The uncertainty in the host and nuclear luminosities, then, is dominated by the measurement process and is 0.12 magnitudes.

The observed underlying host galaxies span a range in absolute magnitude from $M_{\rm H}$=−23.0 ( PG 1119+120) to $M_{\rm H}$=−26.1 (3c273), with a mean value of $M_{\rm H}$=−24.4±0.90 and a median of $M_{\rm H}$=−24.3. The H-band luminosities range from 0.4 to 7.5 $L^*$, with a median of 1.3 $L^*$ and a mean of 2.2 $L^*$. This is almost identical to the result found by McLeod and Rieke (1994a,b), who found a mean $M_{\rm H}$=−24.3 for all PG QSOs with $z < 0.3$. McLeod & Rieke split their data into two samples, a high luminosity sample ($M_{\rm total\ B} < -23.1$; Mcleod & Rieke 1994b) and a low luminosity sample ( $M_{\rm total\ B} > -23.1$; Mcleod & Rieke 1994a). These samples had mean H-band luminosities of $M_{\rm H}$=−24.6 and

−23.9, respectively, and they postulated that this implied that high luminosity QSOs were found in high luminosity hosts (McLeod & Rieke 1994b). In this case it is fair to compare the H-band nuclear luminosity to the B-band total integrated luminosity since the B-band luminosity is dominated by the QSO nucleus (see below) and to first order may be taken as indicative of the QSO nuclear luminosity. Unsurprisingly, our data show a strong correlation between B- band nuclear and total luminosity. We do not, however, actually see a correlation between $M_{\rm B}$ and $M_{\rm H}$ in our data, nor is there is any significant correlation between the H-band luminosity of the host galaxy and either the total or nuclear H-band luminosity. Similarly, there is no statistically significant correlation between nuclear and host luminosity in B or I-band, as well. However, we note our small sample size vs. that of McLeod et al. (1995b; 14 vs. 50) which may prevent such a correlation being observed. Even in the data of McLeod et al. (1995b), the effect is sufficiently weak that it requires binning all of the luminosities into just two groups to be detected. There *is* a statistically significant correlation between $K$- band luminosities of the host and nuclei at better than the 0.995 level. This may support the notion that more luminous QSOs are found in more luminous host galaxies. This correlation may break down at short wavelengths, as seen in our data, due to contamination of the host galaxy light by emission from star formation, contamination by the QSO nucleus due to the increasingly poor spatial resolution at short wavelengths, and extinction by dust which is greater at shorter wavelengths. A similar, albeit weaker, result was found by Taylor et al. (1996).

The QSO host galaxies have a median H-band luminosity very similar to that of ULIGs (Paper II, III), but have a mean luminosity and span a total range more similar to that of the warm ULIGs (Paper II). Figure 5 shows the H-band host luminosity cumulative distribution functions (CDFs) of the three samples. We have subtracted from the total integrated emission all of the light attributable to QSO nuclei, putative AGN, and clustered star formation; the residual should only be emission from old starlight. As expected from

their similar median values, all three samples have nearly identical distribution functions below the 80% number fraction. Both the infrared-excess QSOs and the warm ULIGs have identical distribution functions, suggesting that the same underlying population of galaxy luminosities and hence galaxies make up the hosts. While to some extent this is due to the overlap (16% of QSOs, 25% warm ULIGs) between the two samples, removal of the overlap objects leaves the two CDFs still very similar. As was noted in Paper III, the cool ULIG sample seems to have a dearth of the very highest luminosity hosts, and as a result it's CDF deviates from the other two. There are several interpretations: first, and most importantly, the deviation is not statistically significant. Kolomogorov- Smirnov statistics indicate that we can reject the null hypothesis that the cool ULIG sample is drawn from the same underlying population as the warm ULIG and QSO samples at only the 50% level, mostly due to the small number statistics involved. Second, the warm ULIG and infrared-excess QSO samples are truly complete, i.e. they contain every object meeting the selection criteria, while the cool ULIG sample is only *statistically* complete, as it was drawn randomly from a much larger sample of objects meeting the selection criteria. As a result, it consists of only about 30% of the entire cool ULIG population. While the warm ULIG and QSO samples necessarily contain any existing systems with high luminosity hosts, there is a small likelihood that the cool ULIG subsample will fail to contain any such systems. It is of course also possible that this difference in CDFs is actually real, i.e., there is a difference in the populations of the host galaxies. If this were the case, then the distributions of host luminosities are consistent with the infrared-excess QSOs having evolved from warm ULIGs, but that only 80% of the warm ULIG/QSO populations could have evolved from an earlier cool ULIG state. The remaining warm ULIGs and QSOs either arose from a different process, by nature of their massive hosts never passed through a cool ULIG state, or that any such cool state was comparatively short-lived.

Of the 4 QSO hosts with direct evidence for merger activity, 3 have the highest H-band

luminosities in the sample ($L_H > 3.2L^*$; PG 0007+106, Mrk 1014, and PG 1613+658) while the fourth (PG 1411+442) is more nearly 1.3 $L^*$. This is consistent with their interpretation as mergers of two galaxies. The 5 systems that have barred morphologies that may be consistent with minor merger have a mean luminosity of 1.2 L*.

The fraction of the total system luminosity originating in the QSO nucleus is given in Table 3. The average nuclear fraction is (BIHK′)=(0.79, 0.67, 0.60, 0.71)±(0.08, 0.16, 0.15, 0.10). As expected from previous studies (Sanders et al. 1989, McLeod & Rieke 1995), the minimum nuclear fraction occurs near 1 $\mu$m, which is a result of the relative SEDs of QSOs and galaxies. There is a considerable range in nuclear fractions: the QSO nucleus at $H$-band accounts for anywhere from 36% to 85% of the total luminosity. On average, though, the QSO nucleus and the underlying host galaxy are roughly similar in total magnitude at $H$. At shorter wavelengths such as $B$, the QSO nucleus is roughly 4 times more luminous than the host.

### 3.3. Colors

Optical/near-infrared colors were derived for the QSO nuclei. Figures 6 and 7 illustrate the ($B-I$, $I-H$, $H-K'$) colors of the QSO nuclei, using the two rotations of the optical/near-infrared color cube used in Papers II & III. The figures depict in this three-color basis the colors of an instantaneous starburst taken from Bruzual & Charlot (1993; BC95), as well as the effects of a variety of reddening and emission mechanisms: thermal dust emission, a mixed dust and star distribution, and free-free emission. Also shown are the colors of a synthetic optical QSO developed by Surace et al. (1999) based on the properties of the PG sample as a whole, and the effects of reddening it via inclusion of a hot thermal dust emission component. The colors of "warm" ULIGs are shown with an open circle. The mean QSO nuclear colors are ($B-I$,$I-H$,$H-K'$) = (0.99, 1.56, 0.96)±(0.23,

0.52, 0.17). These colors are similar to those found by Elvis et al. (1994) for UVSX (ultraviolet-soft x-ray) QSOs, and seem to continue to support the large observed intrinsic scatter in QSO colors. All of the observed infrared-excess PG QSOs have ($H-K'$) colors redder than those of both the modeled synthetic QSO and derived observationally from the UVSX sample. This reddening is not consistent with any appreciable (>1 $A_V$) foreground dust screen; instead, it is most consistent with varying small contributions (10–20%) at $K'$ from hot (600–1000 K) dust, which has previously been inferred in these QSOs (Sanders et al. 1989 and references therein). This contribution from hot dust is less extreme than that found in the warm ULIGs, and they are therefore found predominantly between the regions in the 3-color diagram occupied by synthetic optical QSOs and the warm ULIGs. Since the IR-excess QSOs have colors intermediate between the "warm" AGN- like ULIGs and the larger population of optically selected QSOs, possibly because a smaller fraction of the luminosity at $K'$ originates in hot dust and any foreground reddening screen is much thinner, this lends support to the idea that the IR-excess QSOs are transition objects and that as they age much of the dust in the vicinity of the active nucleus is dissipated or destroyed.

An alternative explanation for the near-IR excess could be that of a scattering dust geometry which reddens the observed QSO light. That is, scattering increases the escape of blue photons, and decreases the effective extinction at short wavelengths. However, an examination of Figure 7 shows that the reddening of the IR-excess QSOs is almost entirely due to an excess of K′ emission. The reddening law required to produce this would have to be nearly flat (wavelength-independent) at optical wavelengths. In particular, our observations could be reproduced if E(B-I)$\approx$ E(I-H) $\approx$ 0.2 for $A_V$=1. This is a (B-I) color excess roughly four times less than that of the line-of-sight extinction law. This is also smaller by a factor of several than that derived by Calzetti (1997) for starburst galaxies, in which scattering is believed to be important, or modeled by Witt et al. for various realistic

dust geometries with a central source.

Table 4 presents photometry derived for the star-forming knots and other structures seen in some of the QSO hosts. As in Papers I, II, & III, the photometry was compared to the stellar synthesis models of BC95. A model for the stellar (photosphere) colors from an instantaneous starburst with upper and lower mass cutoffs of 125 and $0.1M_{\odot}$ , respectively, was used. The ages derived from the colors are difficult to constrain, however, primarily due to a lack of sensitivity in the near-infrared - the detection limits are too high. In most cases the constraints that can be made indicate young ages for most of the knots ( less than $\approx 10^8$ years). The arc in PG 0007+106, while apparently bluer than it's surroundings, is unconstrained due to a lack of a clear near-infrared detection. The nuclear knot in PG 1119+120 is very red (H- K = 1.25), with a considerable K′ excess compared to stellar colors (H-K=0.2) The knot in the spiral structure of PG 1119+120 appears quite blue and the upper limit at H implies an age of less than 10 Myrs. Generally, the upper limits at H can constrain the stellar population to young ages below 10-100 Myrs (Surace et al. 2000a) Similarly, the knots in PG 1229+204 are similarly blue and have ages of less than 100 Myrs old. The knots in PG 1411+442 are ill- constrained due to large measured uncertainties, but they are also less than 100 Myrs. The nuclear knot (3) has colors similar to many of the star-forming knots seen in the ULIGs (Surace et al. 2000). Finally, the nuclear knot in PG 1613+658 is most prominent at *H*-band. While actually quite red optically (B-I>3.1), its near-infrared colors are typical of stellar colors (H-K′=0.24).

The colors of the host galaxies themselves as determined from the global and nuclear photometry are poorly determined. This is primarily because the nuclei dominate the luminosity, particularly at very long ($> 2\mu$m) and short ($< 0.5\mu$m) wavelengths. Since the average QSO nucleus is anywhere from 1.5 to 4 times more luminous than the host at B, relatively small errors in the determination of the QSO nuclear luminosity result

in disproportionately large uncertainties in the QSO host luminosity. The mean colors of the QSO sample host galaxies (excluding the 3 ULIGs which are also QSOs) so derived are $(B-I,I-H,H-K')$ = (1.66, 1.86, 0.65)±(0.79, 0.65, 0.36) and are marked with a large solid circle in Figure 6 & 7. These colors are appreciably redder at K′ than expected for a normal stellar population. This same result was found by Surace et al. (1998) for the three warm ULIGs that are also PG QSOs. This may be a result of residual QSO light (which is much redder in the near-infrared than starlight) contaminating the colors of the hosts. The surface brightnesses were measured in small apertures at the apparent half-radius point in the host galaxies (these mean surface brightnesses appear in Figure 8). The colors derived from these representative surface brightnesses are $(B-I,I-H,H-K')$ = (2.16, 2.14, 0.65). This is also a considerable $(H-K')$ excess, considering that these values were measured far enough from the nucleus that residual nuclear contamination should be quite small. On the other hand, these colors are also very similar to those observed in the "nuclei" of the cool ULIGs, and may represent a near-infrared excess due to recent star-formation activity (Paper III). McLeod & Rieke (1994a) find a similarly high value of $H-K$ when comparing their results to those of Dunlop et al. (1993). They note, however, that typical K-corrections to normal galaxy colors may result in $H-K\approx0.45$ (their sample being similar in redshift to ours). If this were combined with modest reddening ( $A_V = 1$ magnitude ) and hot dust emission, the observed colors could be accounted for, considering the uncertainties introduced by the host/nucleus decomposition.

## 4. Conclusions

1. Host galaxies were detected in all 17 observed infrared-excess PG QSOs. The one QSO not observed (PG 1202+281) was already known to have an elliptical host. In many cases these galaxies had observable 2-dimensional structure. At least 50% have features indicative

of spiral structure, 56% of which have strong nuclear bars. Twenty-two percent are clearly on-going merger systems, and galaxy interactions may be implicated in as many as 50% of all the QSO systems.

2. The underlying host galaxies have $H$-band luminosities, which are believed to indicative of the size of the underlying old stellar population, ranging from 0.4 $L^*$ to 7.5 $L^*$, with a mean of 2.2 $L^*$. These luminosities are similar to those of ULIGs, although the "cool" ULIGs with no clear evidence for AGN activity seem to lack the most massive hosts exhibited by "warm" ULIGs and QSOs.

3. The QSO nuclei and their host galaxies are similar in total luminosity at $H$-band, but this ratio increases to an average of 4:1 at $B$.

4. The host galaxies have considerable near-infrared excesses. This may be the result of recent star-formation. Derived ages based on the colors of the observed host galaxy features are typically less than 100 Myrs.

5. Contrary to many expectations, QSO host galaxies at low redshift are easiest to detect at optical and not near-infrared wavelengths. This is due primarily to the low background emission of the sky at optical wavelengths coupled with the large projected size of the extended hosts.

The authors would like to thank Aaron Evans for his useful comments on this paper. The authors would like to thank the telescope operators, John Dvorak and Chris Stewart. J.A.S. was supported by NASA grant NAG 5-3370 and by the Jet Propulsion Laboratory, California Institute of Technology, under contract with NASA. DBS was supported in part by JPL contract no. 961566. This research has made use of the NASA/IPAC Extragalactic Database (NED) which is operated by the Jet Propulsion Laboratory, California Institute of Technology, under contract with the National Aeronautics and Space Administration.

## A. Notes on Individual Objects

The following are descriptive notes explaining various features of the individual QSO hosts. These features are most easily seen in the near-truecolor images of Figure 2.

*PG 0007+106 = Mrk 1051 = III Zw 2* — a single tidal arm or arc extends 22 kpc to the north. This arm has several knots of star formation in its far end. Another galaxy is seen directly to the south. Although there is no apparent connecting structure between the two, there does seem to be some extended low surface brightness emission surrounding all of the galaxies in the field, suggesting that perhaps there are multiple interactions.

*PG 0050+124 = I Zw 1* — this is also a "warm" ULIG and is discussed in more detail in Papers I & II. It has two asymmetric spiral arms, both of which have knots of star formation. The galaxy disk is 30 kpc in diameter.

*PG 0157+001 = Mrk 1014* — this QSO is also a "warm" ULIG and is discussed in detail in Papers I & II. The host galaxy is dominated by a tidal arm extending to the NE.

*PG 0838+770* — a strong nuclear bar 22 kpc in projected length runs E-W through the host galaxy. Knots are seen near each end of the bar. A single spiral arm extends clockwise from each end of the bar. The galaxy itself is elongated perpendicular to the axis of the bar, although this may be a projection effect.

*PG 1001+054* — small and uniform, with no distinguishable features.

*PG 1114+445* — the host galaxy is diffuse and uniform, but shows some evidence to the south of having a small, tight spiral arm, suggesting that this is a face-on disk galaxy.

*PG 1119+120* — a very red compact emission source lies inside the host galaxy envelope to the NW; with high spatial resolution it appears tangentially elongated. The host galaxy consists of a tilted central elliptical condensation which may be a 15 kpc long

bar, with an apparent disk 28 kpc in diameter aligned perpendicular to it. There are at least 5 additional smaller galaxies located within a projected distance of 25″ of the QSO.

*PG 1126−041 = Mrk 1298* — an elongated, elliptical host approximately 30 kpc in diameter. There are projections from the nucleus parallel to the long axis of the host which suggest that this may be a bar structure.

*PG 1202+281 = GQ Comae* — we were unable to observe this QSO due to the sensitivity limitations of our fast tip/tilt guider. However, Bahcall et al. (1997) have observed this system with *HST*/WFPC2 and find that the host galaxy appears to be a small elliptical E1 elliptical galaxy.

*PG 1229+204 = Mrk 771 = TON 1542* — a strong nuclear bar 14 kpc in projected length runs NE-SW through this host. A very blue, linear chain of star-forming knots extends nearly perpendicular to the bar axis at one end. Hutchings et al. (1992, 1994, 1995) claim that this is due to tidal disruption with a small companion; however, it seems more likely that these knots are associated with the bar itself, considering that there appears to be a similar blue region visible on the opposite end of the bar (Figure 2).

*PG 1351+640* — no features are discernible in the ground-based images.

*PG 1402+261* — Bahcall et al. (1997) describes this as an SBb(r) spiral galaxy. The *HST/WFPC2* images show a clear bar with very open arms extending from their ends, a morphology common to several other QSO hosts (e.g., PG 0838+770, PG 1119+120). The ground-based images are just capable of showing this structure.

*PG 1411+442* — a tidal loop 88 kpc long extends to the north, then wraps around to the east and extends south. In the model-subtracted image a counter-tail is seen extending south and curving to the west. In the near- infrared, a linear structure is seen extending to the SW from the nucleus which may be a jet. This same jet-like feature can be seen in the

optical images after subtraction of a radial model.

*PG 1415+451* — no distinguishable features.

*PG 1440+356 = Mrk 478* — the galaxy nucleus is elongated NE-SW, and the body of the galaxy is elongated perpendicular to this, a morphology common to many other QSO hosts. There is some faint evidence of shells or arms.

*PG 1613+658* — first described in detail by Hutchings & Neff (1992). A very obvious tidal tail extends 88 kpc to the east. In the near-infrared a second bright peak appears 2.4″ to the NW and is most easily seen at *H*. There is a companion galaxy nearby; it is unclear if it has anything to do with the QSO host since there is no detection of emission linking the two. There is at least one other small galaxy nearby (33″ to the SW).

*PG 2130+099 = UGC 11763 = Mrk 1513 = II Zw 136* — this appears to be a spiral galaxy 30 kpc in diameter and inclined 60° from face-on. The *HST* images reveal the spiral structure in the host which resembles two concentric rings in the ground-based data. There is an odd asymmetry in the NE part of the host, lending to its overall peculiar appearance.

## B. Detectability of QSO Hosts

It is commonly held that near-infrared observations are optimal for detecting QSO hosts (McLeod et al. 1995, Dunlop et al. 1993). This is motivated primarily by the comparative SEDs of typical spiral galaxies and QSO nuclei; the peak of the galaxy SED is very near the minimum of the QSO SED, and therefore H-band observations yield the highest possible contrast between the galaxy host and the QSO nucleus. This was based on the assumption that the greatest difficulty in detecting QSO hosts was trying to differentiate the extended, low-surface brightness galaxy emission from the wings of the PSF of the extremely bright point-like nucleus.

However, our observations run counter to this — it is actually much easier to detect the QSO hosts at shorter wavelengths like B and I-band. Both our observations and those of others (Hutchings & Neff 1992, Hutchings & Morris 1995) indicate that typical QSO hosts are similar in gross properties to most galaxies. At redshifts of $z$<0.16, a typical host galaxy 30 kpc in diameter is likely to be 5–10″ in radius. This is sufficiently large that at a stable site like Mauna Kea under good conditions (0.5″ FWHM at 5000 Å or 0.3″ at 1.6$\mu$m) the wings of the PSF do not extend measurably to such large radii. Therefore, at low redshift ($z < 0.4$) *the limiting factor in QSO host galaxy detection is background noise* (both instrumental and poisson noise from background sky emission). With modern instruments, the poisson noise from the background sky emission is generally higher than the instrumental noise, although eventually flat-fielding errors become significant. The 2 magnitude increase in host galaxy surface brightness from *I*-band to *H*-band cannot offset the 6 magnitude decrease in sky brightness under a dark sky (this increases to a 9 magnitude difference in sky brightness from *B* to *H*). Space-based observations, which have nearly negligible sky brightnesses, would not be so affected; and hence the increase in host luminosity at near-infrared wavelengths would then increase detectability. Although the decrease in spatial resolution at long wavelengths with instruments like NICMOS would in theory decrease detectability versus optical instruments like WFPC2, as noted above the very large spatial scales of the QSO hosts at low redshift effectively renders this point moot. Only at higher redshifts ($z > 0.5$) would this become important.

Another reason for the increase in detectability lies in the relative morphology of galaxies at long and short wavelengths. At near-infrared wavelengths galaxies are relatively smooth, reflecting the distribution of old stars. At short wavelengths galaxies show much more complex morphologies due to emission from young stars and differential extinction by dust. Features such as spiral arms are more easily detected at short wavelengths, and therefore QSO host galaxies are more *recognizable* in filters such as *B* and *I*. At near-infrared

wavelengths the smooth distribution of old stellar light in the host galaxies is more difficult to detect due to confusion with flat- fielding errors, the wings of the QSO nuclear PSF, etc., while at short wavelengths the high spatial frequency features are more easily separated from large-scale extended background variations.

## REFERENCES

Bahcall, J.N., Kirhakos, S., Saxe, D.H., & Schneider, D.P. 1997, ApJ, 479, 642

Bahcall, J.N., Kirhakos, S., & Schneider, D.P. 1995, ApJ, 450, 486

Barnes, J.E., & Hernquist, L. 1992, ApJ, 393, 484

Barnes, J. & Hernquist, L. 1996, ApJ, 471, 115

Bessell, M.S. 1979, PASP, 91, 589

Bekki., K. & Noguchi, M., 1994, A&A, 290, 7

Canada-France-Hawaii Telescope Observer's Manual, 1990, 5-2

Dunlop, J.S., Taylor, G.L., Hughes, D.H., & Robson, E.I., 1993, MNRAS, 264, 455

Elmegreen, D.M., Elmegreen, B.G., & Bellin, A. 1990, 364, 415

Elvis, M.

Gehren, T., Fried, J., Wehinger, P.A., & Wyckoff, S., 1984, ApJ, 278, 11

Gerritsen, J. 1997, PhD. Thesis, Kapteyn Astronomical Institute, Groningen

Goldader, J., Joseph, R.D., Doyon, R., & Sanders, D.B., 1995, ApJ, 444, 97

Goldschmidt, P., Miller, L. La Franca, F., & Cristiani, S., 1992, MNRAS, 256, 65P

Gunn, J.E., *Active Galactic Nuclei*, 1979, (Cambridge University Press: Cambridge), 213

Heckman, T., Armus, L., & Miley, G, 1990, ApJS, 74, 833

Hernquist, L., 1989, Nature, 340, 687

Hodapp, K.W., Hora, J.L., Hall, D.N., Cowie, L.L. et al. 1996, New Astronomy, 1, 176

Hooper, E., Wilkes, B., McLeod, K., Elvis, M., Impey, C.., Lonsdale, C., Malkan, M. and McDowell, J. 1999, ESA SP-427, 427,893

Hutchings, J.B., Crampton, D., Campbell, B., Duncan, D., & Glendenning, B., 1984, ApJS, 55, 319

Hutchings, J.B., Holtzman, J., Sparks, W.B., Morris, S.C., et al. ApJ, 429, L1

Hutchings, J.B. & Morris, S.C. 1995, AJ, 109, 1541

Hutchings, J.B. & Neff, S.G. 1992, AJ, 104, 1

Kellerman, K.I., Sramek, R.A., Schmidt, M., Green, R.F., & Shaffer, D.B. 1994, AJ, 108, 1163

Kim, D-C., 1995, PhD. Thesis, University of Hawaii

Kohler, T., Groote, D., Reimers, D., & Wisotzki, L. 1997, å, 325, 502

Krist, J. 1994, *The Tiny Tim User's Manual*, (StScI: Baltimore)

Kukula, M.J., Dunlop, J.S., Hughes, D., Taylor, G., & Boroson, T., 1997, in *Quasar Hosts*, 1997, (Springer: Berlin), 177

Kukula, M. J., Dunlop, J. S., Hughes, D. H., & Rawlings, S. 1998, MNRAS, 297, 366

Lake, G., Katz, N. & Moore, B., 1998, ApJ, 495, 152

Laine, S. & Heller, C.H. 1999, MNRAS, 308, 557

McLeod, K.K. & Rieke, G.H. 1994a, ApJ, 420, 58

McLeod, K.K. & Rieke, G.H. 1994b, ApJ, 431, 137

McLeod, K.K. & Rieke, G.H. 1995, ApJ, 454, L77

McLure, R.J., Kukula, M.J., Dunlop, J.S., Baum, S.A., O'Dea, C.P., & Hughes, D.H., 1999, MNRAS, 308, 377

Meurer, G. 1995b Nature, 375, 742

Mihos, J.C., & Hernquist, L. 1994, ApJ, 425, L13

Mihos, J.C., & Hernquist, L. 1994b, ApJ, 431, L9

Neugebauer, G., Green, R.F., Matthews, K., Schmidt, M., Soifer, B.T., & Bennett, J. 1987, ApJS, 63, 615

Neugebauer, G., & Matthews, K. 1999, AJ, 118, 35

Neugebauer, G., Matthews, K., & Armus, L. 1995, ApJ, 455, L123

Rown-Robinson, M. 1995, MNRAS, 272,737

Schmidt, M, & Green, R.F. 1983, ApJ, 269, 352

Sanders , D.B., Phinney, E.S.,,Neugebauer, G., Soifer, B.T., & Matthews, K. 1989, ApJ, 347, 29

Sanders, D.B., Soifer, B.T., Elias, J.H., Madore, B.F., Matthews, K., Neugebauer, G., & Scoville, N.Z. 1988a, ApJ, 325, 74

Stockton, A., & MacKenty, J.W., 1987, ApJ, 316, 584

Sulentic, J. 1989, AJ, 98, 2066

Surace, J.A., Sanders, D.B., Vacca, W.D., Veilleux, S., & Mazzarella, J.M., 1998, ApJ, 492, 116 (Paper I)

Surace, J.A., & Sanders, D.B., 1999, ApJ, 512, 162 (Paper II)

Surace, J.A., Sanders, D.B., & Evans, A.S., 2000a, ApJ, 529, 170 (Paper III)

Surace, J.A., Sanders, D.B. ,2000b AJ, in press (Paper IV)

Taylor, G.L., Dunlop, J.S., Hughes, D.H., & Robson, E.I., 1996, MNRAS, 283, 930

Terlevich, R. in *Dynamics and Interactions of Galaxies*, 1989, (Springer-Verlag: Berlin), 465

Toomre, A., & Toomre, J. 1972, ApJ, 178, 623

Veilleux, S., Sanders, D.B., & Kim, D-C. 1997, ApJ, 484, 92

Veilleux, S., Kim, D.-C., & Sanders, D. B. 1999, ApJ, 522, 113

Yee, H.K.C., 1987, AJ, 94, 1461

Wainscoat, R.J. & Cowie, L.L. 1992, AJ, 103, 332

Webster, R.L., Francis, P.J., Peterson, B.A., Drinkwater, M.J., & Masci, F.J., 1995, Nature, 375, 469

Whitmore, B.C., Miller, B.W., Schweizer, F., & Fall, S.M. 1997, AJ, 114, 1797

Woltjer, L. 1990, in Active Galactic Nuclei.

Wright, G.S., Joseph, R.D., Robertson, N.A., James, P.A., & Keikle, W.P.S., 1988, MNRAS, 233, 1

This manuscript was prepared with the AAS LaTeX macros v4.0.

Fig. 1.— BIHK′ data for the infrared-excess PG QSO sample. Image intensities have a log scaling to accentuate the low surface brightness features in the host galaxies. The B and I-band data have been smoothed by convolution with a 0.36″gaussian kernel. Ticks are every 2″, with major ticks every 10″. The scale bar is 10 kpc. NE is at top left.

Fig. 2.— Near-truecolor images of the QSO sample constructed from the B & I-band data. The galaxy SEDs have been linearly interpolated from the $B$ and $I$ data; the color balance is not absolute. For completeness, I Zw 1 and Mrk 1014 have been included from Paper I. 3C273 and PG 1202+281 do not appear since B & I observations of these QSOs were not obtained.

Fig. 3.— Archival images of infrared-excess PG QSOs taken with *HST*/WFPC2 in the V and R filters as part of other programs (Bahcall et al. 1997, Hutchings & Morris 1995). Tick marks are 1″, and the physical scale bar is 10 kpc.

Fig. 4.— Enhanced images of PG QSOs showing small-scale structure. All of the images have had a radial model of the QSO light subtracted from them, except for the bottom right, which has been deconvolved with the Richardson- Lucy algorithm. The middle right panel is a close-up of the middle left panel showing the emission very close to the QSO nucleus. The location of the QSO nucleus in all cases is marked with a cross; the structure within a few arcseconds of this location (except in the middle panel) is residual error from the PSF subtraction. Tick marks are 1″.

Fig. 5.— Cumulative distribution functions of the host galaxy luminosity at H-band for the three ULIG and QSO samples.

Fig. 6.— ($B-I$,$I-H$,$H-K'$) color cube illustrating the colors of the QSO nuclei. For clarity, the QSO nuclei have been marked with numbers: (1) PG 0007+106 (2) PG 0838+770 (3) PG 1001+054 (4) PG 1114+445 (5) PG 1119+120 (6) PG 1126-041 (7) PG 1229+204 (8)

PG 1351+640 (9) PG 1402+261 (10) PG 1411+442 (11) PG 1415+451 (12) PG 1440+356 (13) PG 1613+658 and (14) PG 2130+099. The mean host galaxy colors are given by the large filled circle. The cube is rotated to be orthogonal to the reddening vector, which is depicted by the closed boxes and represents line-of-sight extinction, i.e. a simple foreground dust screen, in units of $A_V = 1$ magnitude. It is derived from Rieke & Lebofsky (1985). The median colors of the "warm" ULIGs are marked with a large circle. The open circles are the colors of an instantaneous starburst with a Salpeter IMF and mass range 0.1–125$M_\odot$ and aging from 0 to 15 Gyrs, based on the spectral synthesis models of Bruzual & Charlot (1993; an updated version called BC95 is used here). The large dotted open circle is a synthetic QSO spectrum based on multiwavelength observations of all Palomar-Green QSOs and is discussed in detail in Paper II. It is indicative of the colors of typical optically selected quasars. The closed circles illustrate an 800K thermal dust contribution to the colors of the optically selected QSOs and to a 100 Myr-old starburst. The joined, open circles show the effects of adding free-free emission with a 20,000 K electron temperature in increments of 20% of the total flux at K′ to the starburst. The two sets of filled, joined circles illustrate emission from 800 K dust contributing in increments of 10% to the total flux at K′. Finally, emission from uniformly mixed stars and dust, in units of $A_V$=10, 30, and 50 magnitudes, are shown by the $\times$ symbol. One $\sigma$ error bars are shown at upper right. Note that the line-of-sight dust extinction and thermal dust emission curves are nearly orthogonal. The QSO nuclei are very similar to the synthetic QSO colors and "warm" ULIGs.

Fig. 7.— Same as Figure 6, but rotated as to be parallel to the reddening vector. Most of the QSO nuclei have colors similar to the synthetic QSO colors, albeit with high values of ($H$–$K'$). This near-infrared excess, however, is less than that of the warm ULIGs.

Fig. 8.— A comparison of the surface brightnesses of the night sky (closed circles) on Mauna Kea (CFHT Observer's Manual 1990; Wainscoat & Cowie 1992) vs. the observed

mean surface brightnesses of QSO host galaxies (open circles) as a function of wavelength. The surface brightnesses were measured at the apparent half radius of the galaxies. Host galaxies are easier to detect at optical wavelengths such as $I$ due to the much lower sky brightness.

TABLE 1

DETAILS OF IR-EXCESS PG QSO OBSERVATIONS

| Name | RA (J2000.0) | DEC (J2000.0) | z | $L_{ir}/L_{blue}$ | Inst.[a] | Exposure Times (sec) B | I | H | K′ |
|---|---|---|---|---|---|---|---|---|---|
| PG 0007+106 | 00:10:31.0 | 10:58:29.5 | 0.089 | 0.48 | QT | 2280 | 2520 | 1980 | 1980 |
| PG 0838+770 | 08:44:45.6 | 76:53:09.4 | 0.131 | 0.66 | QT | 1920 | 2520 | 2520 | 1800 |
| PG 1001+054 | 10:04:20.1 | 05:13:00.5 | 0.161 | 0.48 | QT | 2680 | 840 | 2160 | 2040 |
| PG 1114+445 | 11:17:06.4 | 44:13:32.6 | 0.144 | 0.98 | QO | 1440 | 1080 | 540 | 720 |
| PG 1119+120 | 11:21:47.1 | 11:44:18.3 | 0.050 | 0.69 | QT | 1080 | 1860 | 1680 | 1440 |
| PG 1126−041 | 11:29:16.7 | −04:24:07.6 | 0.060 | 0.79 | QT | 2340 | 1860 | 900 | 1080 |
| PG 1202+281 | 12:04:42.2 | 27:54:11.4 | 0.165 | 1.04 | W | ... | ... | ... | ... |
| PG 1229+204 | 12:32:03.6 | 20:09:29.2 | 0.064 | 0.54 | QH | 1200 | 960 | 2040 | 1440 |
| PG 1351+640 | 13:53:15.8 | 63:45:44.8 | 0.088 | 0.81 | QT | 2280 | 1800 | 1440 | 1560 |
| PG 1402+261 | 14:05:16.2 | 25:55:33.7 | 0.164 | 0.55 | WQT | 3240 | 1800 | 2400 | 1200 |
| PG 1411+442 | 14:13:48.4 | 44:00:13.6 | 0.090 | 0.69 | QO | 1440 | 1200 | 1200 | 2220 |
| PG 1415+451 | 14:17:00.6 | 44:56:06.4 | 0.114 | 0.73 | QH | 1200 | 1440 | 2280 | 2400 |
| PG 1440+356 | 14:42:07.5 | 35:26:22.9 | 0.079 | 0.83 | QT | 1500 | 1680 | 1500 | 1920 |
| PG 1613+658 | 16:13:57.2 | 65:43:09.6 | 0.129 | 1.25 | QT | 900 | 720 | 2100 | 2700 |
| PG 2130+099 | 21:32:27.8 | 10:08:19.5 | 0.062 | 0.52 | WQT | 2340 | 1260 | 2640 | 2400 |

[a]Q = UH2.2m f/31 QUIRC, T = UH2.2m f/31 Tektronix 2048, H = UH2.2m f/31 Orbit reimaged at f/10 through HARIS spectrograph, O = UH2.2m f/31 Orbit, W = *HST*/WFPC2

TABLE 2

GLOBAL AND NUCLEAR PHOTOMETRY OF IR-EXCESS PG QSOs

| Name | Morph.[a] | $M_B^b$ | $m_B$ | | $m_I$ | | $m_H$ | | $m_{K'}$ | |
|---|---|---|---|---|---|---|---|---|---|---|
| | | | Int. | Nuc. | Int. | Nuc. | Int. | Nuc. | Int. | Nuc. |
| PG 0007+106 | M | −22.0 | 15.77 | 16.2 | 14.30 | 15.1 | 11.81 | 12.5 | 10.78 | 11.3 |
| PG 0838+770 | SB | −22.4 | 16.28 | 16.6 | 15.12 | 15.7 | 13.32 | 14.4 | 12.66 | 13.3 |
| PG 1001+054 | ? | −23.0 | 16.15 | 16.2 | 15.50 | 15.6 | 14.48 | 14.8 | 13.41 | 13.8 |
| PG 1114+445 | S | −22.8 | 16.06 | 16.2 | 14.78 | 14.9 | 13.34 | 14.2 | 12.32 | 12.9 |
| PG 1119+120 | SB | −21.4 | 15.09 | 15.3 | 13.55 | 14.3 | 12.19 | 12.6 | 11.63 | 11.8 |
| PG 1126-041 | SB | −22.0 | 14.92 | 15.1 | 13.53 | 14.0 | 11.92 | 12.3 | 11.12 | 11.3 |
| PG 1202+281 | E | ... | ... | ... | ... | ... | ... | ... | ... | ... |
| PG 1229+204 | SB | −21.5 | 15.55 | 16.0 | 13.96 | 15.1 | 12.33 | 13.2 | 11.72 | 12.4 |
| PG 1351+640 | ? | −23.1 | 14.63 | 14.8 | 13.65 | 13.9 | 12.74 | 13.0 | 11.89 | 12.1 |
| PG 1402+261 | SB | −23.7 | 15.51 | 15.8 | 14.98 | 15.1 | 13.22 | 13.4 | 12.07 | 12.3 |
| PG 1411+442 | M | −23.0 | 14.79 | 15.1 | 13.88 | 14.1 | 12.42 | 12.9 | 11.67 | 12.1 |
| PG 1415+451 | ? | −22.5 | 15.90 | 16.2 | 14.70 | 15.2 | 12.98 | 13.4 | 12.14 | 12.6 |
| PG 1440+356 | S | −22.4 | 15.15 | 15.3 | 13.77 | 14.1 | 11.83 | 12.2 | 11.08 | 11.4 |
| PG 1613+658 | M | −23.0 | 15.67 | 16.1 | 13.98 | 14.5 | 12.19 | 13.0 | 11.44 | 12.1 |
| PG 2130+099 | S | −22.4 | 14.56 | 14.8 | 13.48 | 14.0 | 11.63 | 12.0 | 10.78 | 11.0 |

[a] Host Galaxy Morphology: M=Merger, S=Spiral, ?=Indeterminate, E=Elliptical, B=Barred. Additionally, we classify the following ULIGs: I Zw 1 = S, Mrk 1014 = M, 3C273 = E

[b] Uncertainties in total system measurements are 0.05 magnitudes, and for nuclear and host galaxy measurements are 0.12 magnitudes.

TABLE 3

NUCLEAR LUMINOSITY FRACTION IN PG QSOs

| Name | B | I | H | K′ |
|---|---|---|---|---|
| PG 0007+106 | 0.67 | 0.47 | 0.52 | 0.61 |
| PG 0838+770 | 0.77 | 0.57 | 0.36 | 0.58 |
| PG 1001+054 | 0.97 | 0.93 | 0.74 | 0.70 |
| PG 1114+445 | 0.90 | 0.88 | 0.46 | 0.58 |
| PG 1119+120 | 0.80 | 0.49 | 0.71 | 0.83 |
| PG 1126−041 | 0.82 | 0.65 | 0.39 | 0.82 |
| PG 1202+281 | ... | ... | ... | ... |
| PG 1229+204 | 0.64 | 0.36 | 0.44 | |
| PG 1351+640 | 0.84 | 0.78 | 0.79 | 0.81 |
| PG 1402+261 | 0.78 | 0.92 | 0.85 | 0.82 |
| PG 1411+442 | 0.78 | 0.80 | 0.65 | 0.68 |
| PG 1415+451 | 0.73 | 0.65 | 0.69 | 0.68 |
| PG 1440+356 | 0.88 | 0.71 | 0.72 | 0.77 |
| PG 1613+658 | 0.70 | 0.60 | 0.46 | 0.53 |
| PG 2130+099 | 0.83 | 0.61 | 0.72 | 0.79 |

TABLE 4

DETAILS OF PG QSO SMALL STRUCTURE

| Name | Δ RA[a] | Δ Dec | Aperture[b] | $m_B$ | $m_I$ | $m_H$ | $m_{K'}$ |
|---|---|---|---|---|---|---|---|
| | arcseconds | | | | | | |
| PG 0007+106 arc | −2.8 | 6.4 | 5.0 | 20.80 | 18.37 | >15.80 | >17.60 |
| PG 1119+120 knot 1 | −0.7 | 2.8 | 1.0 | >19.10 | 16.93 | 16.64 | 15.39 |
| PG 1119+120 knot 2 | 9.5 | −1.0 | 1.0 | 22.30 | 21.25 | >20.70 | >20.70 |
| PG 1229+240 SW knots | -4.1 | -4.1 | 0.9 | 20.78 | 19.37 | >18.80 | >18.80 |
| PG 1411+442 knot 1 | 3.5 | −18.6 | 1.0 | 23.53 | 20.70 | >20.70 | >20.20 |
| PG 1411+442 knot 2 | −0.2 | 8.3 | 1.0 | 22.07 | 20.13 | >20.00 | >20.10 |
| PG 1411+442 knot 3 | −1.1 | −1.7 | 1.0 | 20.18 | 18.91 | 16.35 | 15.88 |
| PG 1613+658 knot | −2.4 | 0.7 | 1.0 | >22.80 | 19.74 | 15.95 | 15.71 |

[a] offsets given relative to the QSO nucleus.

[b] aperture radius in arcseconds.

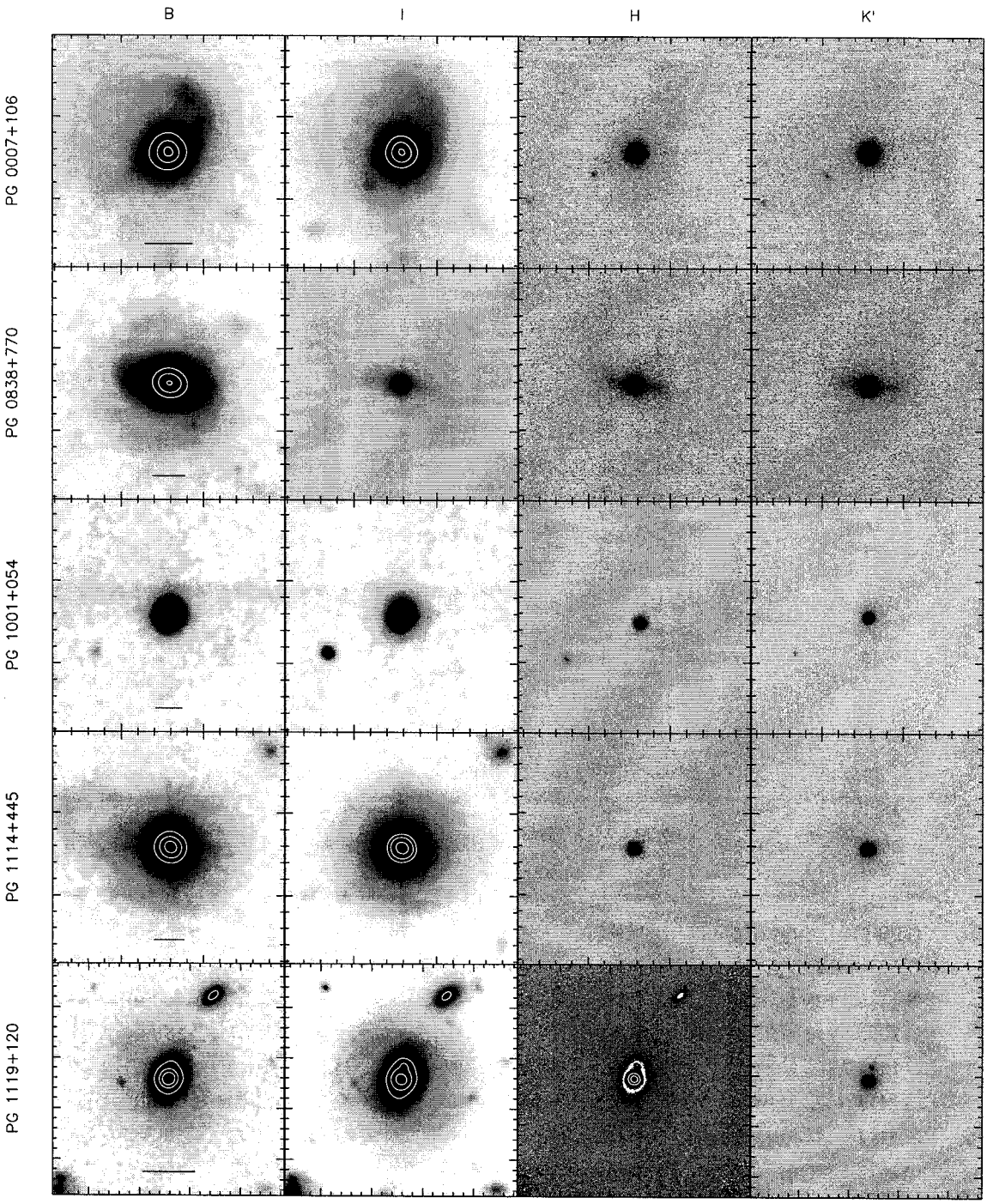


Fig. 1.—

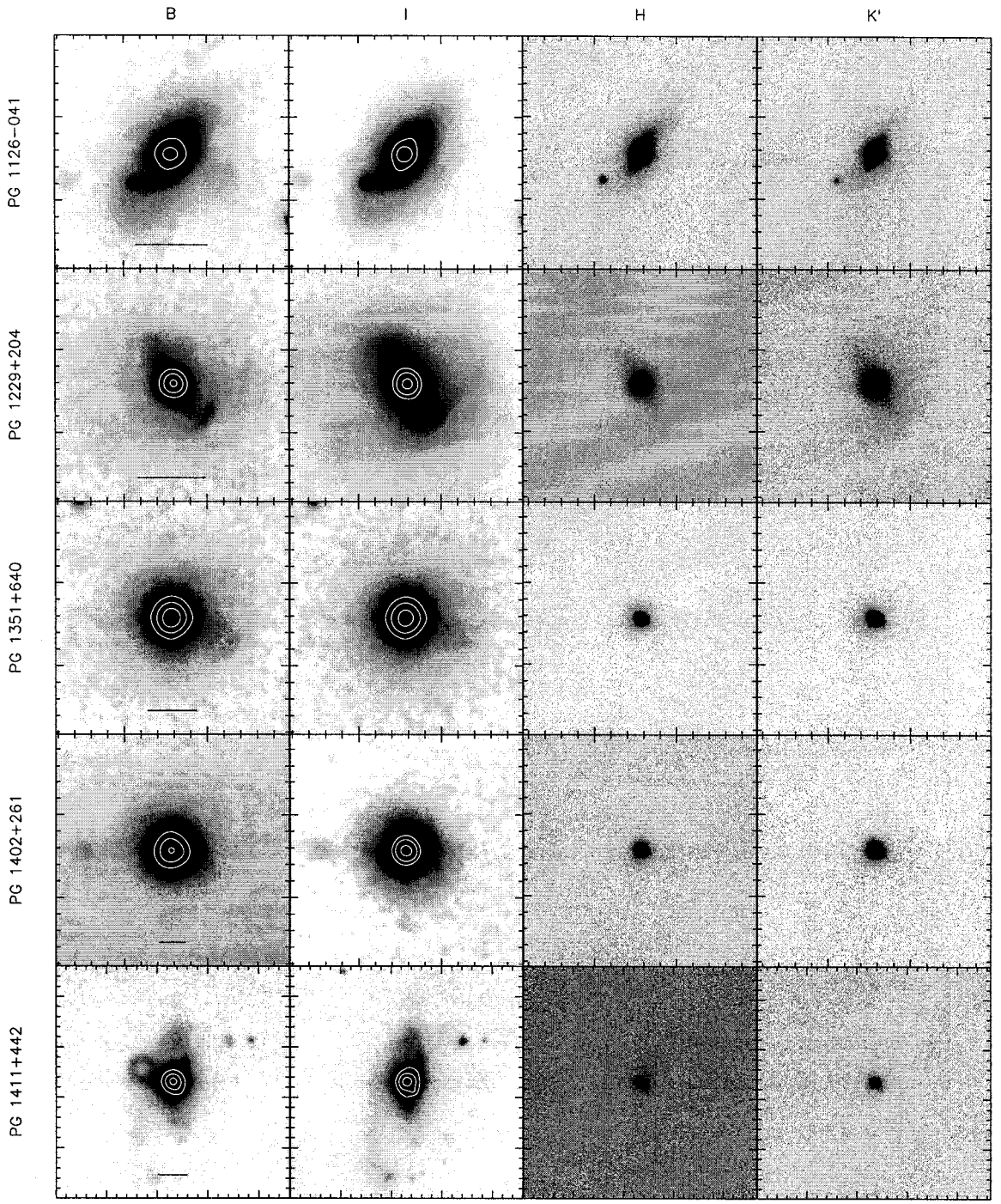


Fig. 1.—

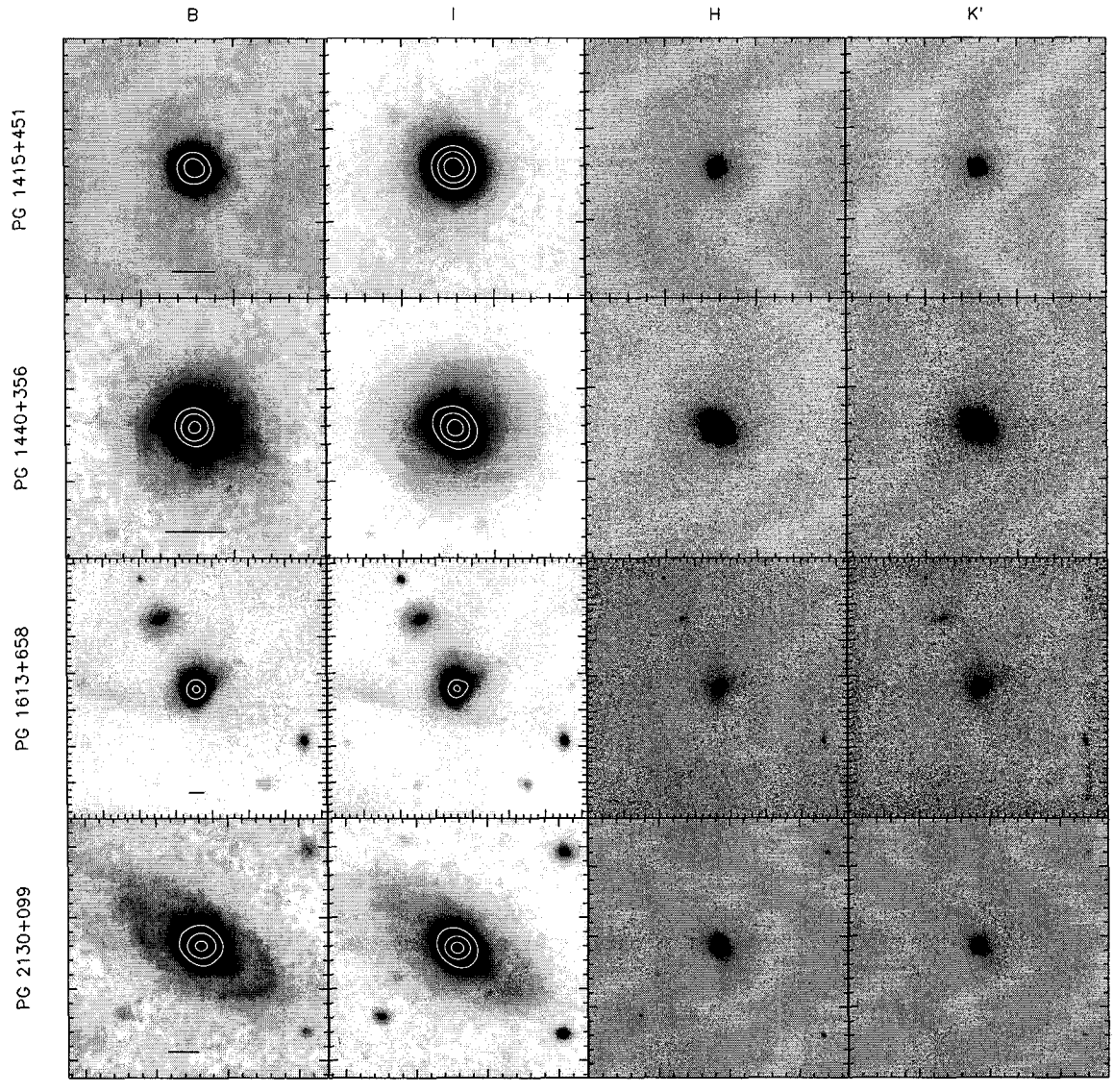


Fig. 1.—

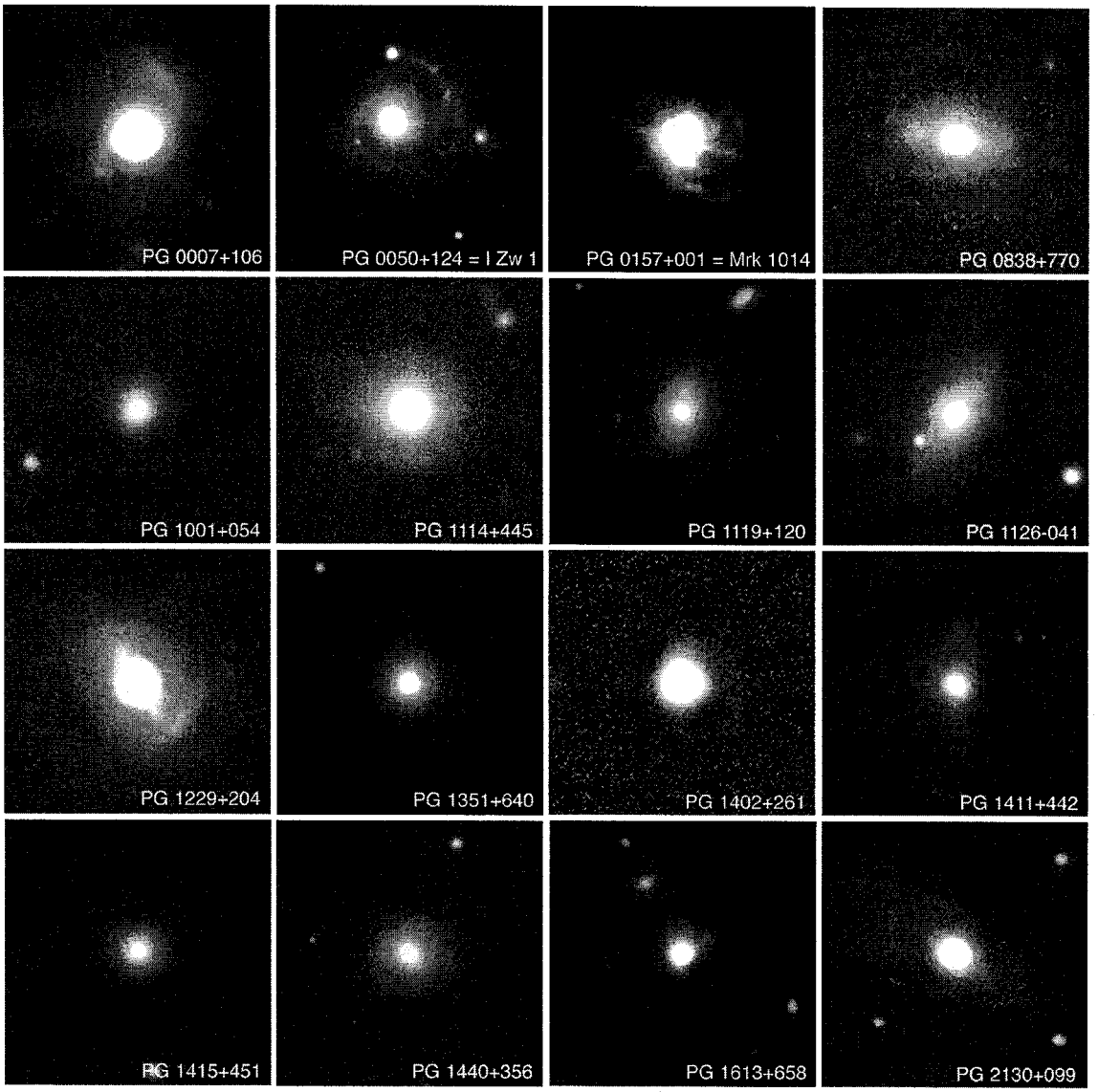
PG 0007+106
PG 0050+124 = I Zw 1
PG 0157+001 = Mrk 1014
PG 0838+770
PG 1001+054
PG 1114+445
PG 1119+120
PG 1126-041
PG 1229+204
PG 1351+640
PG 1402+261
PG 1411+442
PG 1415+451
PG 1440+356
PG 1613+658
PG 2130+099

Fig. 2.—

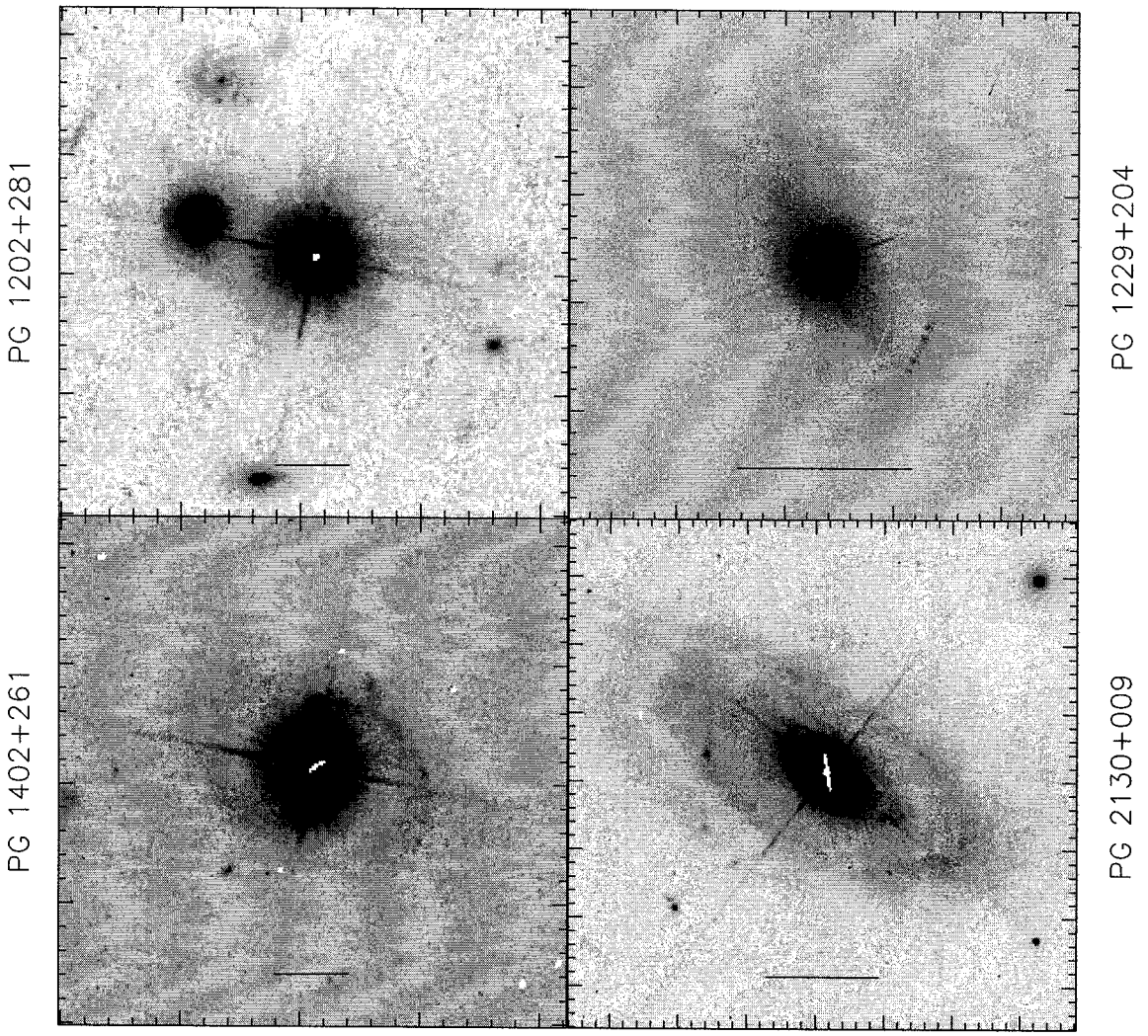


Fig. 3.—

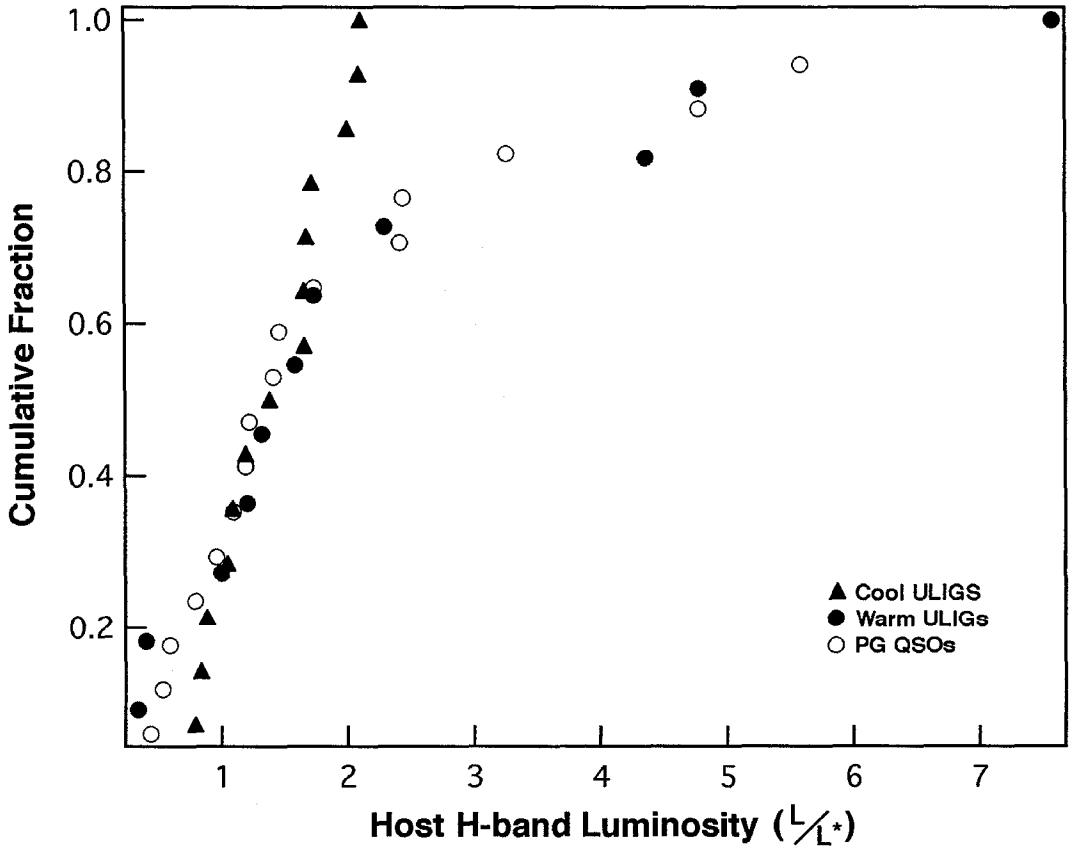
1.0
0.8
0.6
0.4
0.2
Cumulative Fraction
1
2
3
4
5
6
7
Host H-band Luminosity (L/L*)
Cool ULIGS
Warm ULIGs
PG QSOs

Fig. 4.—

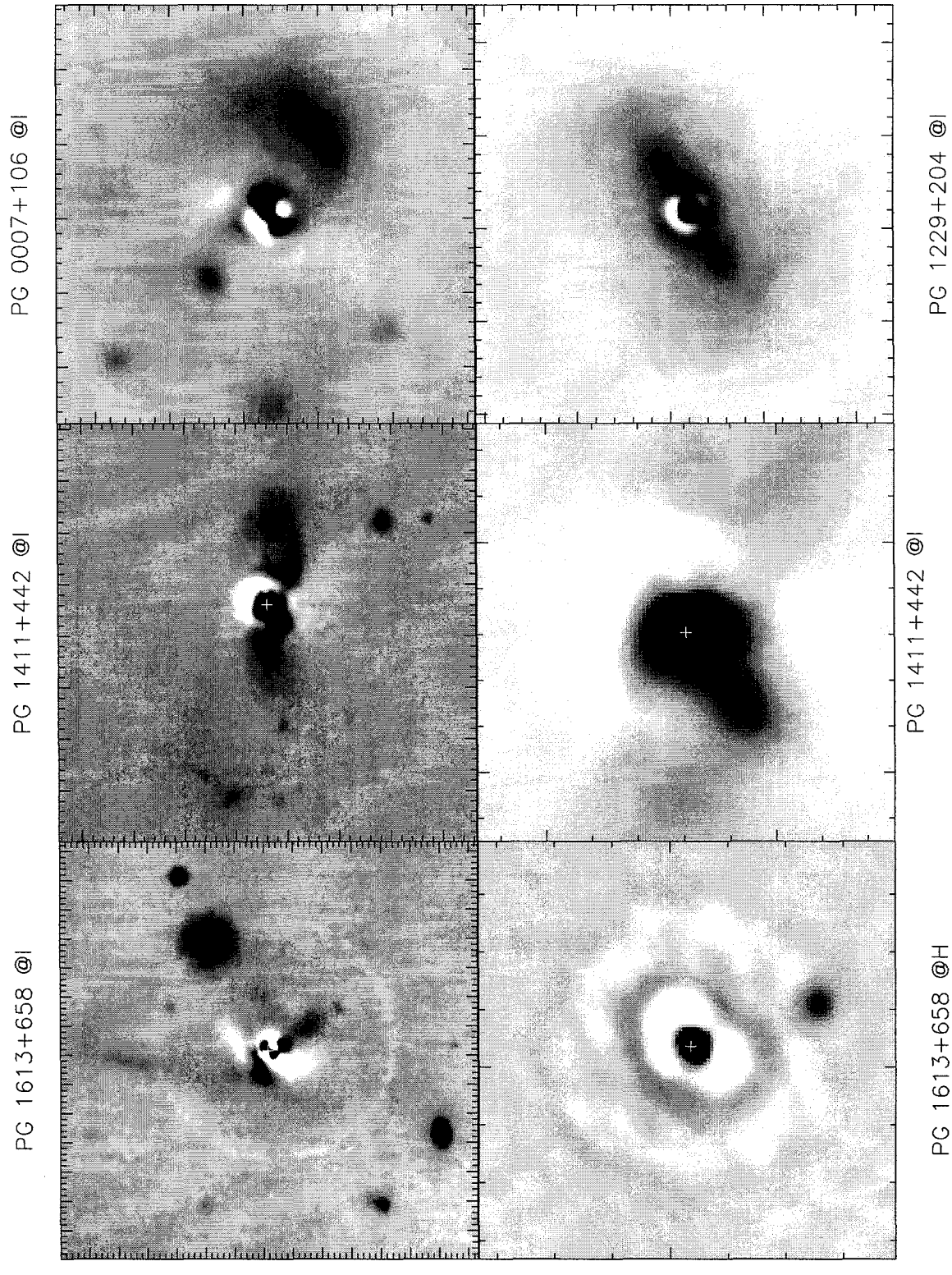
PG 0007+106 @I
PG 1411+442 @I
PG 1229+204 @I
PG 1613+658 @I
PG 1411+442 @I
PG 1613+658 @H

Fig. 5.—

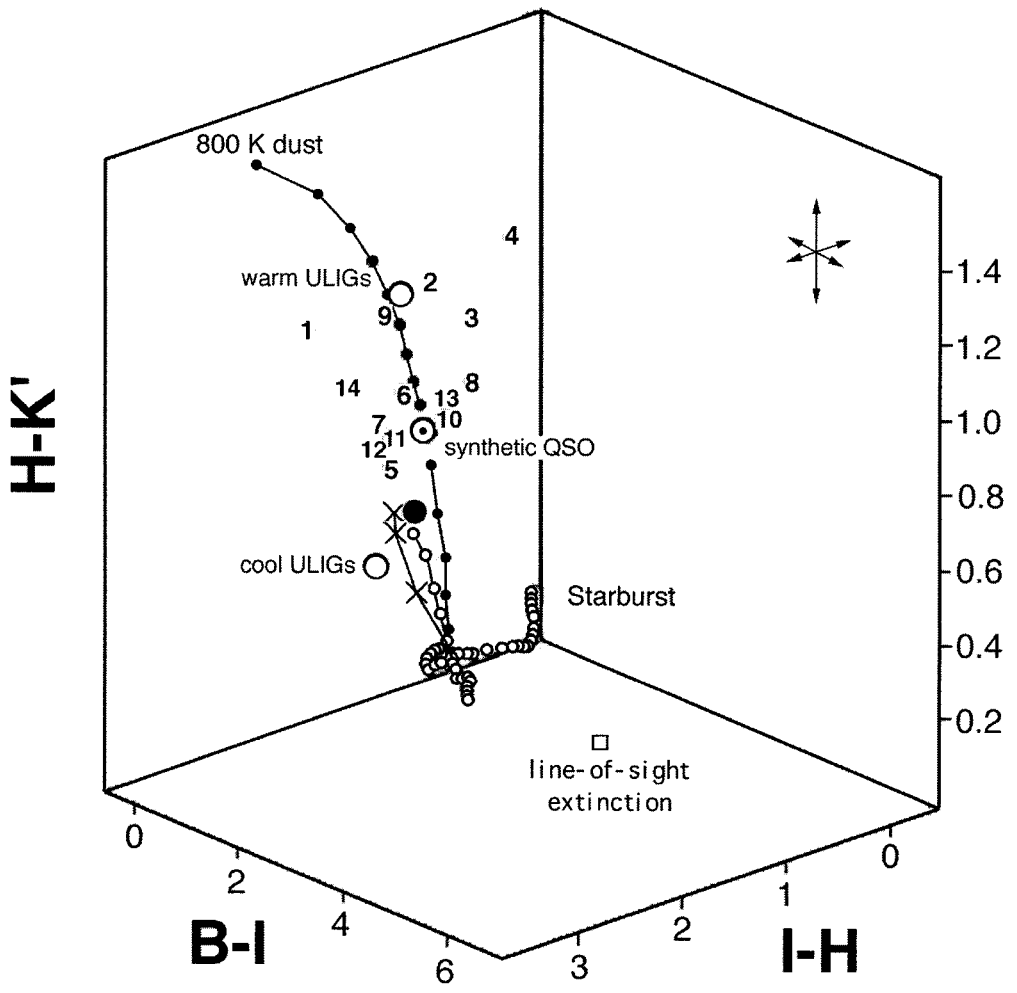
800 K dust
warm ULIGs
synthetic QSO
cool ULIGs
Starburst
line-of-sight
extinction
H-K'
B-I
I-H
1.4
1.2
1.0
0.8
0.6
0.4
0.2
0
2
4
6
3
2
1
0

Fig. 6.—

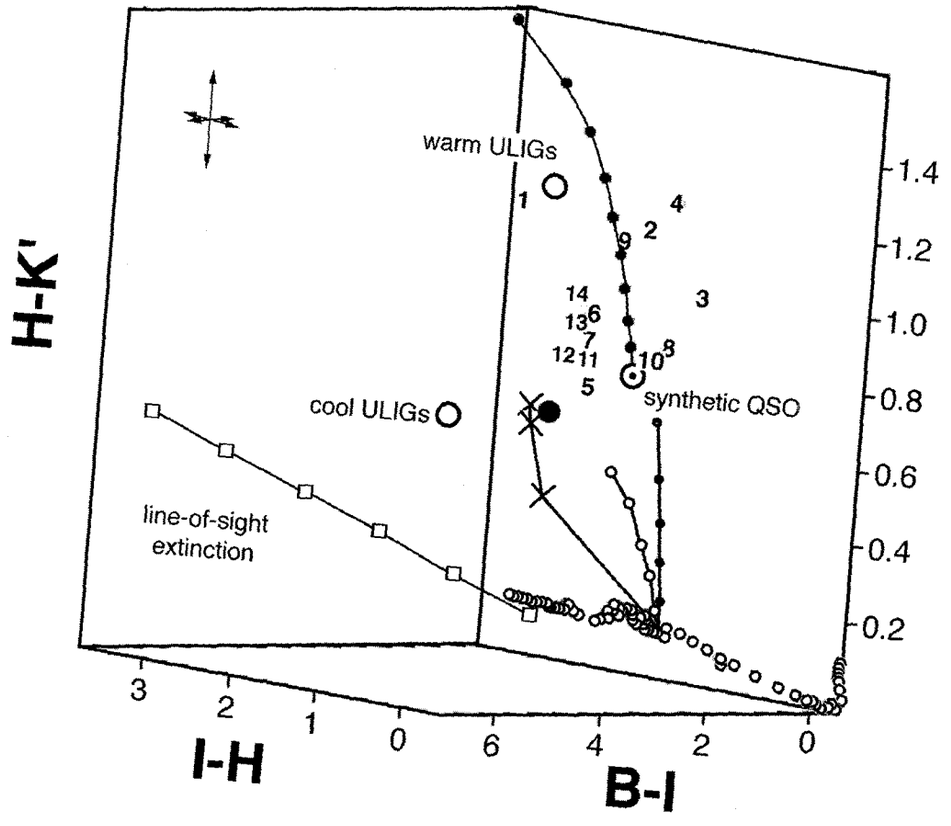
H-K'
warm ULIGs
cool ULIGs
synthetic QSO
line-of-sight
extinction
1
2
3
4
5
6
7
8
9
10
11
12
13
14
1.4
1.2
1.0
0.8
0.6
0.4
0.2
3
2
1
0
I-H
6
4
2
0
B-I

Fig. 7.—

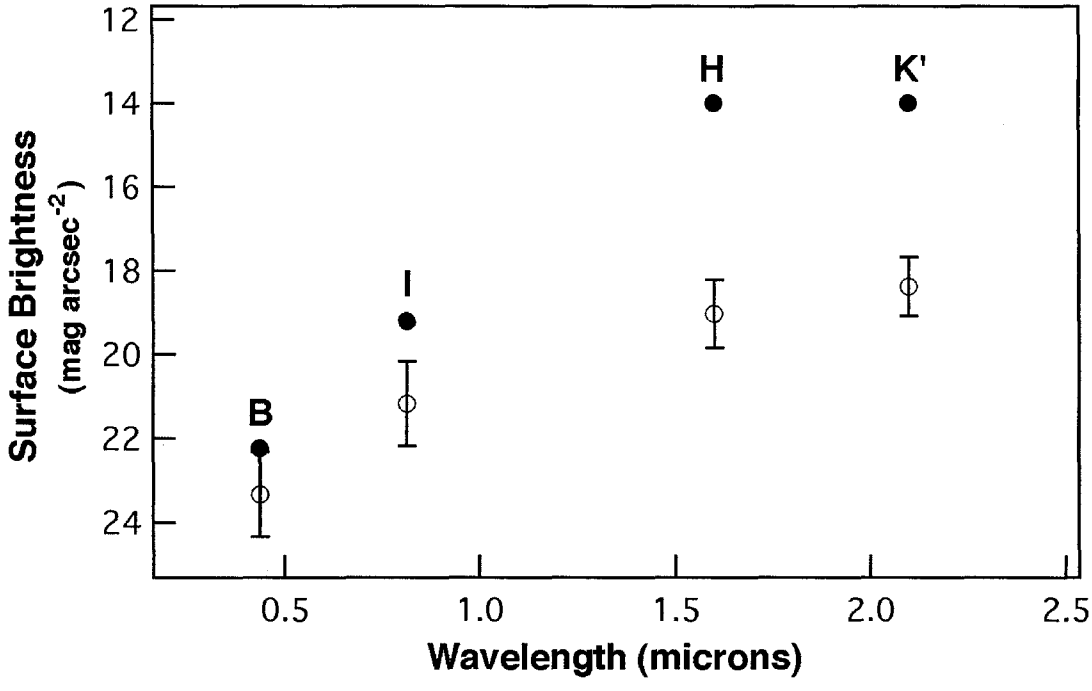
12
14
16
18
20
22
24
Surface Brightness
(mag arcsec$^{-2}$)
B
I
H
K'
0.5
1.0
1.5
2.0
2.5
Wavelength (microns)

Fig. 8.—